Investigation of the influence of the temperature on the fracture properties of adhesive joints using the Arcan device

Vincent Dumont, Georgios Stamoulis, C. Badulescu, A. Lefèvre, David Thévenet

Version of Record: https://www.sciencedirect.com/science/article/pii/S0013794422002636
Manuscript_6d64beece75a03566a3979ce107be33d

Investigation of the influence of the temperature on the fracture properties of adhesive joints using the Arcan device

V. Dumont[1,3,*], G. Stamoulis[2], C. Badulescu[1], A. Lefèvre[3], and D. Thévenet[1]

[1]ENSTA Bretagne, UMR CNRS 6027, IRDL, F-29200 Brest, France

[2]Univ. Bretagne Occidentale, UMR CNRS 6027, IRDL, F-29200 Brest, France

[3]Safran Reosc - Engineering & Integration Department - 91280 St Pierre-du-Perray, France

March 8, 2022

Keywords: Structural bonding; Fracture mechanics; Temperature effect; Arcan; Fracture energy

Corresponding author: *vincent.dumont@ensta-bretagne.org*

Abstract

The evolution of the mixed mode I+II fracture envelope of a structural epoxy adhesive was investigated here, under three different temperatures: -15, 23 and 45°C. The study was performed using the Arcan device, by improving a previously published methodology to calculate the critical strain energy release rate (G_C). For the range of temperatures that was examined, the shape of the fracture envelopes remained similar. However, G_C was found to decrease with the increase of the temperature. This was attributed to the energy intake of the adhesive material, since its glass transition temperature was measured at 88°C (much higher than 45°C).

Nomenclature

a	Crack length
a_0	Initial crack length
b	TDCB specimen width
C	TDCB system compliance
CTE	Coefficient of Thermal Expansion
CZM	Cohesive Zone Models
DIC	Digital Image Correlation
DSC	Differential Scanning Calorimetry
F	Load reached during crack propagation (TDCB tests)
FE	Finite Element
F_{exp}	Experimental load during Arcan tests
$F_R(U, a)$	Reaction force for an imposed displacement field U and a crack length of a
G	Energy release rate or fracture energy
G_{IC}	Mode I critical strain energy release rate
G_{IIC}	Mode II critical strain energy release rate
G_C	Critical strain energy release rate
$\frac{G_{II}}{G}$	Mode ratio
HLS	High Limit of elasticity Steel
J	Contour integral
LEFM	Linear Elastic Fracture Mechanics
m	Dimensionless hlGong-Benzeggagh parameter
MMB	Mixed mode Bending
MPC$Link$	Multiple Point Constraints of type link
R_1 and R_2	Regions used on Arcan samples for the DIC
RP	Reference Point ($Abaqus^{TM}$)
TDCB	Tapered Double Cantilever Beam
T_g	Glass transition temperature
$\mathbf{T}$	Traction vector used for the calculation of J
$\mathbf{u}$	Displacement
$u^{\vec{z}}_{R_i}$ and $u^{\vec{y}}_{R_i}$	Normal and tangential displacements of R_1 and R_2
W	Strain energy density used for the calculation of J
$(\vec{X}, \vec{Y}, \vec{Z})$	Unit vector of the Cartesian coordinate system used in the study
γ	Arcan angle
Γ	Contour around the crack tip
$\boldsymbol{\varepsilon}$	Strain tensor
$\boldsymbol{\sigma}$	Stress tensor

1 Introduction

A wide range of industrial fields nowadays rely on structural bonding and adhesively bonded assemblies for various reasons, such as their contribution in building lighter and therefore more energy-saving structures. Furthermore, this technique allows for multi-materials assembling, and features fairly good stress distribution properties. Among these fields, one may mention aeronautics, marine systems or automotive, each one being extremely careful regarding the mechanical strength of their structures. The tools of fracture mechanics, developed since the beginning of the 19^{th} century [1], make it possible to answer most of the questions about the ruin of such bonded assemblies for several loading states. These tools allow researchers to measure the critical strain energy release rate or fracture toughness (G_C) of the adhesive, which defines the potential energy dispelled during the propagation of a crack within a material. This critical strain energy release rate is entirely linked to the loading direction with respect to the crack propagation plane (commonly referred to as modes): mode I (the tensile opening mode), mode II (the in-plane shear mode) and mode III (the out-of-plane shear mode). For the needs of the present research, only modes I and II are of interest. For investigations regarding the mode I critical strain energy release rate (G_{IC}) of an adhesive, one would use DCB (Double Cantilever Beam) or TDCB (Tapered Double Cantilever Beam) specimen geometries. Both of these methods have already been standardized for adhesives [2–4] and have been extensively used in previous research [5]. Unfortunately, there are no standardized methods to investigate mode II and mixed-mode $I + II$ load cases for adhesive joints. It is nonetheless possible to export standards from the composite materials field to adhesive joints, such as the Mixed Mode Bending (MMB) test [6], or the End Notch Flexure (ENF) test [7]. These methods, once adjusted for structural adhesives, have been shown to produce satisfying results [8–10]. Yet, some minor issues have been reported for the case of bi-material composite-metal joints [11]. In order to process the raw results from these tests (TDCB, MMB etc.), one may use the Linear Elastic Fracture Mechanics (LEFM) framework to extract the fracture properties of the considered adhesive material.

Based on the industrial applications briefly discussed above, adhesive joints may be exposed to severe environmental conditions during operation; these mainly involve changes in temperature and/or relative humidity. Due to the polymeric nature of structural adhesives, their mechanical behaviour shows an important viscous character [12]. Therefore, it is reasonable to assume that the mechanical behaviour along with the fracture properties of adhesives are impacted by the working environmental conditions. Examples of the evolution of the mechanical properties of adhesive joints with the temperature can be found in [13–15]. For the needs of the study presented in this paper, only the dependence of the fracture energy (G) on the temperature will be examined. Some studies in the past showed a decrease of the G_{IC} values of adhesive joints with the increase of temperature until about 50°C [16–18]. However, the mode II critical strain energy release rate (G_{IIC}) was found almost unaffected from the thermal ageing procedure in [17]. On the other hand, G_{IC} was found to considerably increase when increasing the testing temperature to 80°C in [18]; this was attributed to the increase of the ductility at the crack tip for temperatures close to the glass transition temperature (T_g), which was measured equal to 125°C for the adhesive examined in that study. The evolution of G_{IC} and G_{IIC} in a wide range of temperatures for two polyurethane

adhesives can be found in [19] and [20] respectively. In these last studies, both G_{IC} and G_{IIC} showed a peak around the T_g, then decreased with the increase of the temperature when outside that area. It is interesting to mention that all previous results for G_{IC} and G_{IIC} found in literature were obtained after analyzing the measured fracture data by means of the LEFM theory. A significant impact on the values of G in the mixed mode $I+II$ plane was calculated when considering the non-linear behaviour of a structural epoxy adhesive (Sikapower®-498), for tests performed at ambient temperature in [21].

To the authors knowledge, until the writing of the present article, no influence of the temperature on full fracture envelopes of adhesive joints in the mixed mode $I+II$ plane is reported in literature. Yet, one could assume that G_C under mixed mode $I+II$ loading should vary with the temperature similarly to the pure mode G_{IC} and G_{IIC} reported by several research teams; some of the latter results were briefly presented just before. Nonetheless, the authors decided to investigate the impact of temperature change on the full fracture envelope of a structural bi-component epoxy adhesive submitted to mode $I+II$ load. In particular, three temperatures were examined: -15, 23 and 45°C. The adhesive chosen for the needs of the present research is aimed to be used for bonding optical components mounted in systems like space-based telescopes, satellites and spacecrafts. These components are often thermally regulated in order to guarantee their optical performances throughout operational lifetime. Thus, the three aforementioned temperatures were chosen to cover the range of these regulated thermal environments. Unfortunately, despite the contrary will of the authors, the trade name of the adhesive under investigation cannot be communicated for reasons of confidentiality related to the industrial partner or the project. However, the results presented here should be representative for structural epoxy adhesives tested at temperatures far from their T_g.

In order to answer to the problematic described in the previous paragraph, in the next sessions, the fracture envelope of the adhesive under investigation was firstly identified by means of standardized TDCB and MMB tests at room temperature (23°C). Secondly, the modified Arcan device [22] was put into use by means of a specially designed specimen geometry, so as to perform the same study in a more unusual approach. The implementation of the Arcan fixture was decided mainly due to the fact that the TDCB-MMB specimen and experimental fixtures, respectively, were unable to fit in the thermal chamber used here to perform the tests under temperature, due to their large dimensions. The authors present in §3.3.1 a full methodology to analyze the data issued from the modified Arcan fixture and calculate the G_C of the investigated adhesive under mixed mode $I+II$ load. This consists of an improvement of the previously published method in [23] for the Sikapower®-498 adhesive, where detailed visual inspection of the specimen during testing was necessary to identify the point in the experimental force-displacement curve to which the computation for G_C was to be done. The results for G_C calculated from the TDCB-MMB tests and from Arcan based experimental data at room temperature were almost identical (similarly to the findings for the Sikapower®-498 adhesive in [23]). Hence, the measurement of the fracture envelopes of the adhesive under investigation in the other two temperatures (of -15 and 45°C) was carried out by means of the Arcan fixture. The analysis of all experimental data at all three temperatures that were examined was based on the LEFM theory. The TDCB-MMB and Arcan specimen preparation, testing

procedure, data analysis and results, are exposed in the first and second parts, respectively, of the present article.

2 Part I: TDCB-MMB tests at room temperature

In the following study, the room temperature is considered to be 23°C, as it was checked during the corresponding experiments.

2.1 Preparation of the specimens

The specimens hereafter described were designed to investigate the fracture properties of an epoxy structural adhesive at room temperature using TDCB and MMB tests. All of the samples consisted of two metal substrates bonded by a 0.4 mm thick adhesive layer. The bonding surfaces of the substrates, no matter the geometry, were treated in order to guarantee the best possible adhesion properties. First, they were mechanically ground with 180 grit Silicon Carbide sandpaper, to remove any oxide layer that may have formed during the storage of the substrates and to create an adequate surface roughness for the bonding. Then, they were cleaned using 99% pure acetone, in order to remove any oily and/or greasy compounds on the surfaces, which may be due to the machining or the handling of the metal pieces. Finally, they were dried using compressed air. The elastic mechanical properties of the substrates can be found in Table 1.

	Young's modulus [GPa]	Poisson's ratio [-]	Yield stress [MPa]
Aluminum 2017A	72.5	0.33	280
High Limit of elasticity Steel (HLS), Raex 450	210	0.33	1200

Table 1: Some mechanical properties of the metallic alloys used for the substrates [8].

The adhesive investigated in this study is a bi-component epoxy adhesive, whose trade name cannot be communicated for confidentiality reasons (as also mentioned in the Introduction section). A few general properties of this adhesive are presented in Table 2.

Property	Value
Young modulus's [GPa]	1.4
Poisson's ratio [-]	0.33
Glass transition temperature (T_g) [°C]	88°C

Table 2: General properties of the structural bi-component adhesive under investigation.

2.1.1 TDCB samples

The TDCB samples consisted of two Aluminium 2017A substrates (see Table 1) of varying cross-section Fig. 1. They were bonded using a special fixture previously published in [24], in order to guarantee proper

alignment between the substrates and a uniform thickness of the adhesive joint.

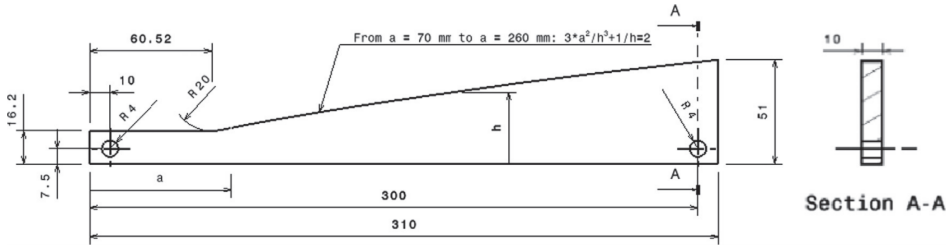

(a) TDCB substrates design

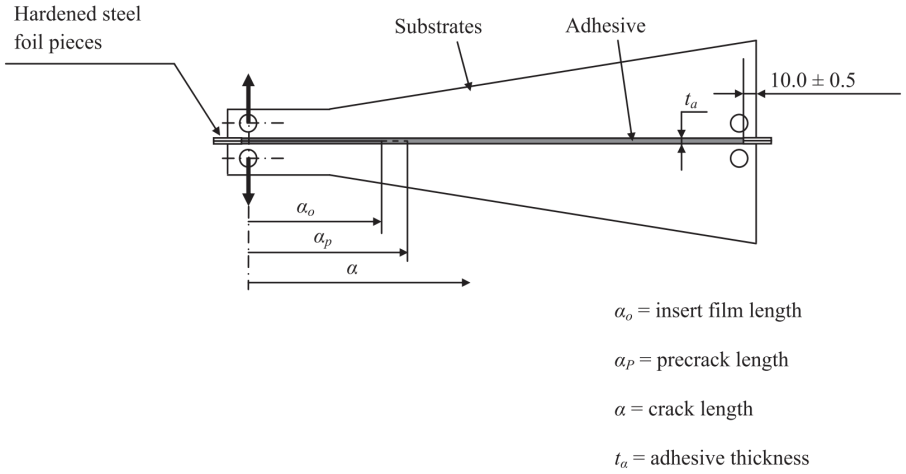

(b) Bonded TDCB sample

Figure 1: TDCB samples geometry and loading principle [8]

2.1.2 MMB samples

The MMB samples were made of HLS steel (Raex 450) substrates (see Table 1), to prevent plasticization during the tests. Loading blocks were glued onto them (Fig. 2a), so the samples could be placed in the loading apparatus developed by Reeder and Crews [25] (Fig. 2b). This apparatus can be used to load the specimens according to various mode ratios, by adjusting the lever arm length c (Fig. 2b). The value of c corresponding to a given mode ratio can be determined using the guidelines of the ASTM D6671 standard [6]. Values of interest for c can be found in [8, 24]. The bonding setup for the MMB specimens previously described in [24] was used in this study to bond the substrates, for the same reasons as described above in §2.1.1 for the TDCB specimens.

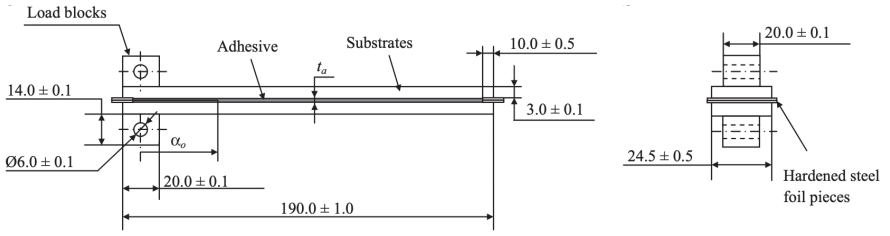

(a) MMB samples design

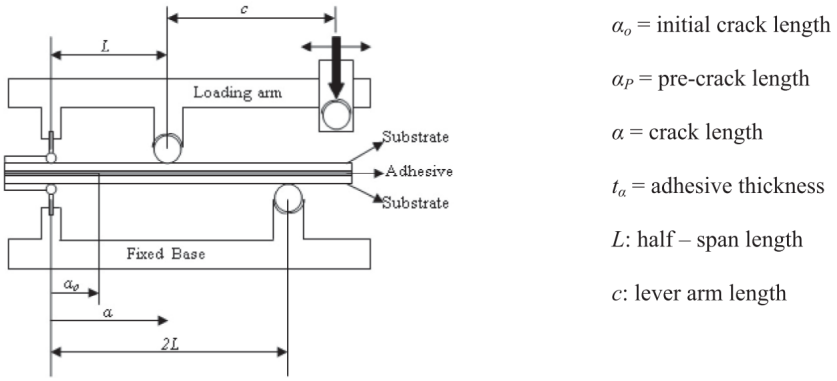

(b) MMB test design and dedicated loading apparatus

Figure 2: MMB samples geometry and loading principle [8]

2.1.3 Bonding and curing

The components of the epoxy adhesive (hardener and resin) were mixed together following the ratio specified by the manufacturer using a planetary mixer. A layer of adhesive was spread onto the bonding surface of each substrate, which were then assembled as described before in §2.1.1 and §2.1.2 for the TDCB and MMB cases respectively. A 50 µm thick polyamide film was placed at the loading end of the samples (Figs. 1b and 2b), in order to create an initial crack. The initial crack length values (a_0), measured from the load-line as shown in Figs. 1 and 2, are given in Table 3 for both geometries.

Sample type	a_0 [mm]
TDCB	70.5
MMB	35.0

Table 3: Pre-crack lengths for the different sample geometries used in this study.

The samples were then placed in a Memmert UF110+™ oven for the curing process. The thermal cycle consisted of four steps (Fig. 3a): i) a 24h long isothermal step at 23°C, ii) a 0.7°C.min^{-1} ramp until 80 °C, iii) a second isothermal step at 80°C for 2h and iv) a 0.2°C.min^{-1} cooling ramp to room temperature. This cycle has been validated by Differential Scanning Calorimetry (DSC) measurements (Fig. 3b) realized on the adhesive under investigation before and after curing; it resulted in a polymerization rate between

95% and 97%. A thermocouple was also placed in the middle of the joint of a spare sample in order to monitor the temperature within the adhesive. As it may be seen in Fig. 3a, no significant deviation was observed between the imposed and measured temperatures. Once the curing cycle completed, the samples were removed from the thermal enclosure to let them arrive at room temperature, and any excess of adhesive that may have dripped on the sides of the samples was removed by grinding with 180 grit sandpaper.

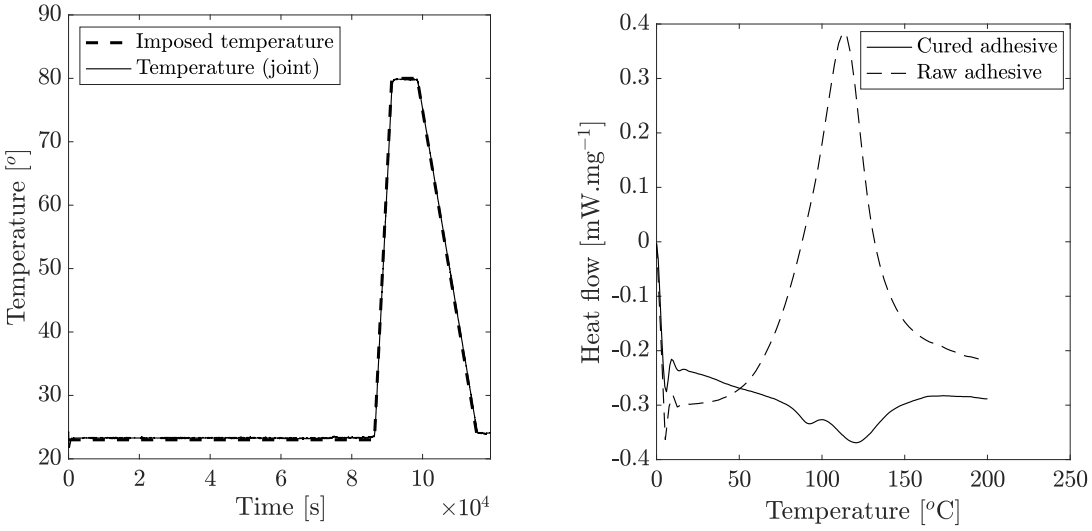

(a) Adhesive curing cycle

(b) DSC curves of raw and cured samples of the adhesive under investigation

Figure 3: Curing of the adhesive

2.2 Experimental procedure

For the mode I load case (TDCB), a total of eight specimens were investigated to ensure good repeatability of the results. For the mixed mode $I + II$ load case, four different mode ratios $\frac{G_{II}}{G}$ were investigated by means of the MMB fixture: 0.2, 0.4, 0.6 and 0.8; for each mode ratio, three samples were tested. Both TDCB and MMB tests were realized by means of an MTS universal tension-compression machine under displacement control at 0.4 mm/min. All specimens were first loaded then unloaded to properly detach the insert used to fabricate the initial crack from the surrounding bulk adhesive material and create a sharp crack tip. All results that will be presented in §2.3 are those after the previously described procedure. The TDCB samples were loaded until failure; the MMB samples were loaded until the crack reached the middle contact point of the specimen with the loading arm (Fig. 2b), since any exploit of the MMB test results after this point is meaningless [24]. For all tests, crack propagation was monitored by means of a high resolution Retiga™ 6000 camera. During the TDCB tests, the relative displacement between the machine grips was measured by means of a 3D digital image correlation GOM™ system in order to perform the necessary stiffness corrections. During the MMB tests, the same system was used to monitor the opening and rotation of the specimens at their left extremity (that is at the left contact point with the loading arm, Fig. 2b). Indicatively, the installation of the TDCB samples on the MTS

machine is given in Fig. 4.

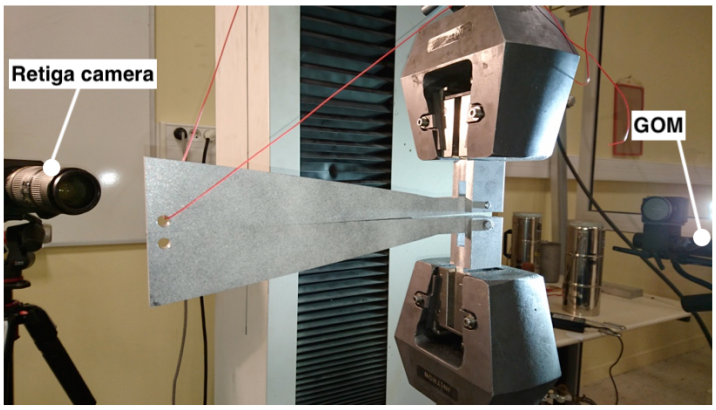

Figure 4: TDCB sample installation on the MTS tension-compression machine

2.3 Test results at room temperature

2.3.1 TDCB

The experimental curves obtained from the TDCB tests are given in Fig. 5a. The curves show that the force increases linearly until it reaches a plateau value, slightly below 1200N. The little differences at the initial slope can be attributed to the differences of the initial crack length values after the load-unload procedure described in §2.2. In addition, the graphs witness that crack propagation was globally stable, except for sample 2 where a tiny instability appeared in the beginning of the plateau. The faces of rupture after the TDCB tests were cohesive; an example is exposed in Fig. 5b.

The TDCB test results were processed using the LEFM theory, as advised by the corresponding ISO standard [4]. According to the standard, the fracture energy can be calculated by means of the Irwin-Kies equation [26], which mathematically reads

$$G_C = \frac{F^2}{2b}\frac{dC}{da} \tag{1}$$

where $G_C = G_{IC}$, F is the force at a certain displacement level during the crack propagation phase, b is the width of the samples and $\frac{dC}{da}$ is the rate of change of the compliance of the assembly C with respect to the crack length a. Due to the particular geometry of the TDCB samples and to their varying cross-section, the evolution of C versus a should be linear. Therefore, according to the [4] standard, the following equation is valid

$$\frac{dC}{da} = constant \tag{2}$$

By measuring the crack length using the Retiga™ 6000 camera (Fig. 4), the C versus a plot was found indeed linear (Fig. 6). The slope $\frac{dC}{da}$ to be used in the Irwin-Kies equation (Eq.1) was directly obtained

by fitting a first-order polynomial through the experimental (a, C) couples (Fig. 6). By doing so, its value was calculated at 2.47e-05 N^{-1}.

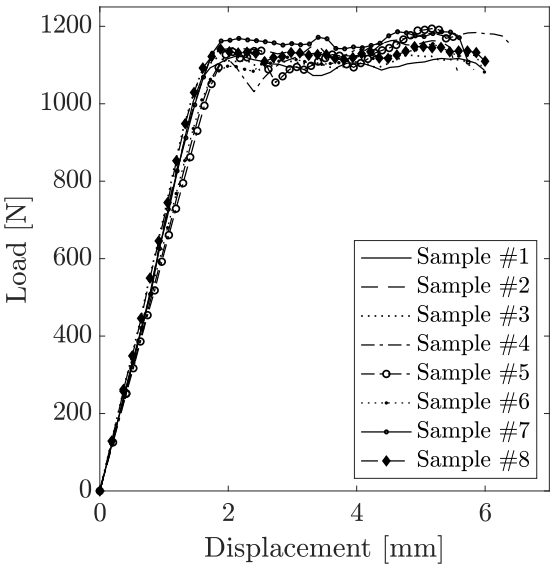

(a) TDCB load-displacement curves

(b) TDCB fractured sample

Figure 5: TDCB test results

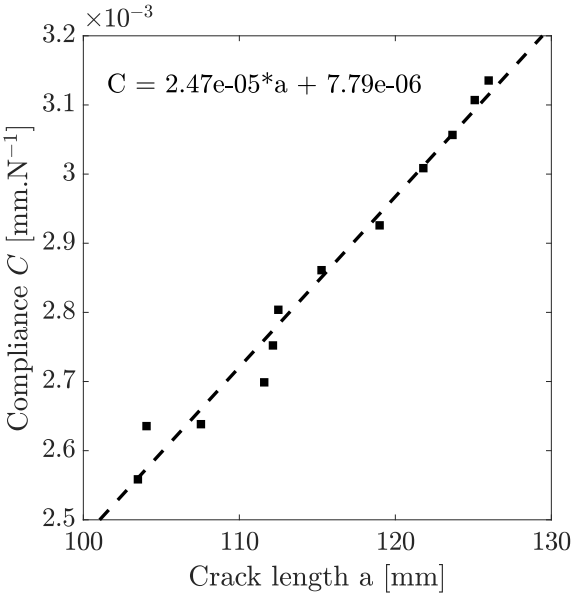

Figure 6: Experimental determination of $\frac{dC}{da}$

For each sample, the average load reached during the plateau (Fig. 5a) was extracted in order to compute the value of G_{IC} by means of Eq. (1). The results of this operation are shown in Table.4. It can be

concluded that the mean value for G_{IC} was around 1.58 kJ/m^2 for the adhesive under investigation.

Sample	G_{IC} [kJ/m^2]
TDCB-1	1.54
TDCB-2	1.67
TDCB-3	1.66
TDCB-4	1.66
TDCB-5	1.65
TDCB-6	1.50
TDCB-7	1.60
TDCB-8	1.49
Mean	1.58
Standard deviation	0.07

Table 4: G_{IC} computation for each TDCB sample

2.3.2 MMB

Fig. 7 illustrates the experimental curves issued from the MMB tests performed for the adhesive under investigation at $\frac{G_{II}}{G} = 0.2, 0.4, 0.6$ & 0.8. The graphs show that the force increased linearly until a maximum, then rapidly dropped to lower values. This phenomenon indicates that after crack initiation the crack propagated unstably at all mode ratios. The MMB tests were stopped just after this rapid fall of the value of the force. Since the MMB samples were not brought to total failure, no picture of the faces of rupture is available. Nonetheless, as the crack during the MMB tests tends to propagate towards the upper substrate [24] (the term upper refers to the substrate in contact with the loading arm, Fig. 2b), similar behaviour can be assumed for the adhesive under investigation here too.

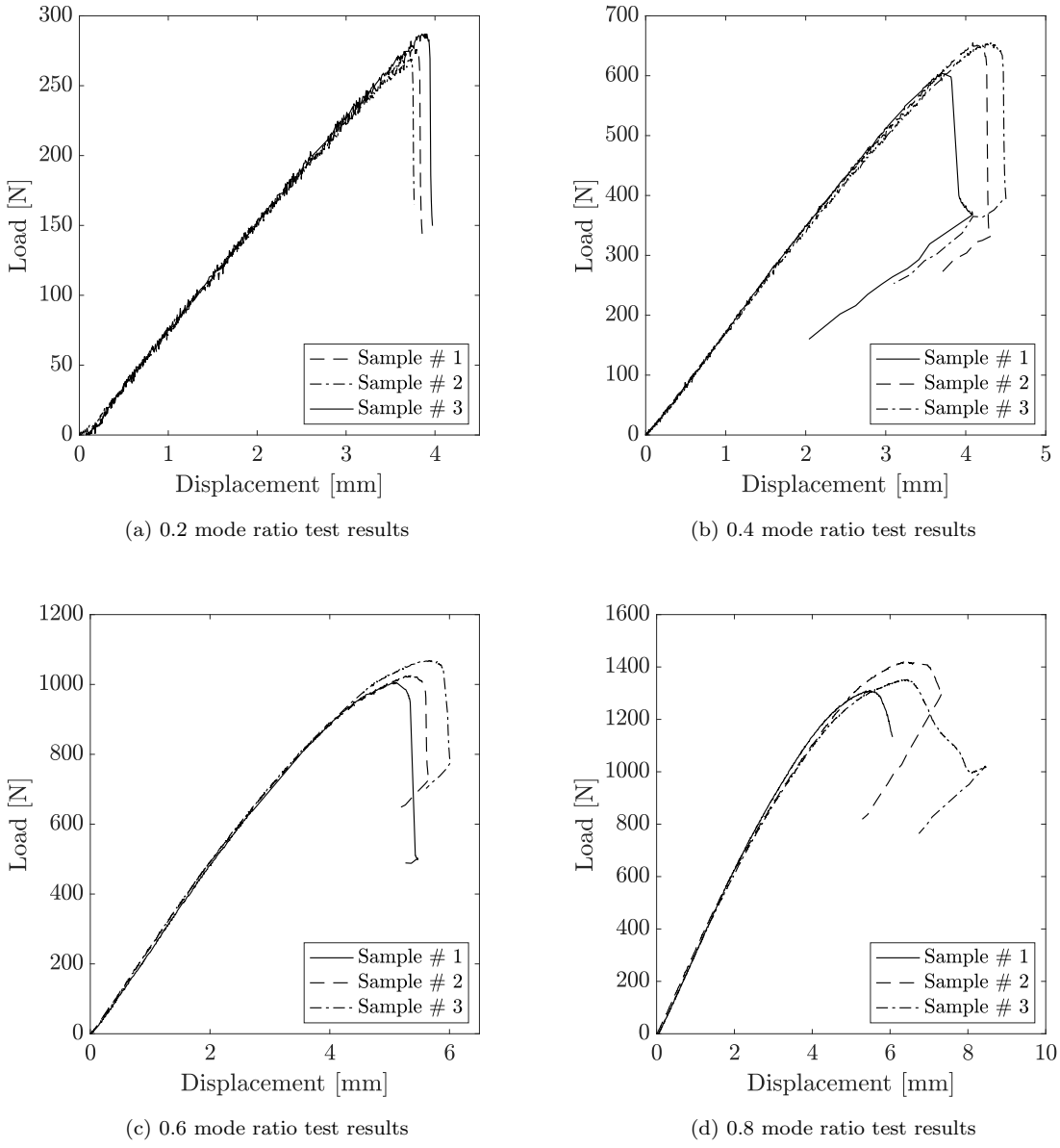

(a) 0.2 mode ratio test results

(b) 0.4 mode ratio test results

(c) 0.6 mode ratio test results

(d) 0.8 mode ratio test results

Figure 7: MMB test results

The computation of G_C for these MMB test results was based on the J-contour integral calculation [27, 28], using Finite Element (FE) modeling. Since FE modeling was implemented, the mechanical properties of the MMB substrates given in Table 1 were considered in the computations of the fracture energy. Hence, no discrepancy of the values of G_C is expected due to the substrates material mismatch between the TDCB and MMB samples (aluminium and steel respectively). The same methodology to calculate the fracture envelope has also been successfully used in previous works [8, 24]. The contour integral, also known as the Rice-Eshelby integral [29], is defined by

$$J = \int_{\Gamma} \left(W dy - \mathbf{T} \frac{\partial \mathbf{u}}{\partial x} ds \right) \tag{3}$$

where Γ is an arbitrary counterclockwise curve which fully contains the crack tip, W is the strain energy density defined by $W = \int \boldsymbol{\sigma} d\boldsymbol{\varepsilon}$ ($\boldsymbol{\sigma}$ and $\boldsymbol{\varepsilon}$ being the stress and strain tensors, respectively), $\mathbf{T} = \boldsymbol{\sigma} n$ is the traction vector (n being the vector normal to Γ) and ds is the differential of the curvilinear abscissa along Γ. Under the assumptions of the LEFM theory $J = G_C$, since no other energy dissipation mechanism is involved. The value of the J-integral computed from Eq.3 is independent from the chosen Γ path [27]. Since the MMB test was modeled here by means of FE, the domain contour integral method was finally used to calculate G_C, which is simply the numerical implementation of the J-contour integral [30].

The modeling technique used in this study was similar to the work done in [8, 24], in terms of contact definitions, interactions and meshing. In particular, the model was created in Abaqus™v.2017. An overview is shown in Fig. 8. The loading arm (Fig. 2b) was supposed non-deformable for the range of forces that were examined. Hence, it was modeled by means of beam connectors of infinite rigidity. The substrates and the adhesive were considered under linear elasticity. The mechanical properties of the substrates material (HLS steel, Raex 450) used in the model were those provided by the supplier (Table 1). Those of the adhesive were measured by means of Arcan tests at 0°and 90°, and are presented in Table 2. Both the substrates and the adhesive layer were meshed under plain strain assumption with CPE4 linear quadrilateral elements. To gain in computational time, the mesh density of the substrates and the adhesive layer was adjusted after a mesh convergence study: i) the finest mesh was used for the adhesive, ii) a less dense mesh for the upper substrate and iii) a coarser mesh for the down substrate (upper is the substrate in contact with the loading arm and lower the one in contact with the machine frame). The mesh of the upper substrate was denser compared to the down substrate because the former one strains more compared to the latter one during an MMB test [24]. Since non-homogenous mesh between the adhesive and the substrates was used, the up and down surfaces of the adhesive were *tied* with the corresponding faces of the up and down substrates respectively. The term *tie* in Abaqus means that the surfaces involved have the same degrees of freedom when the structure is deformed. This technique has shown reliable results in the past when analyzing MMB test results to compute G_C [8, 24]. The contact of the specimen with the loading arm at the middle (up substrate) and the machine frame (down substrate) were considered as hard and frictionless (the default options to define contacts in Abaqus™). The connexion with the loading block at the left extremity of the loading frame was simulated as a Multiple Point Constraint (MPC) of type *Link* (in Abaqus™ MPC*Link* results to a rigid connexion of the nodes involved with the control point, 'RP4' in Fig. 8b, allowing only the rotation around that point). The crack was represented by the *seam crack* option of Abaqus™, which simply doubles the nodes along the segments involved and results to free crack faces with no interaction properties. The crack was supposed in the middle of the adhesive layer. A circular crack front of 0.3 mm was considered (Fig. 8c); this circular path was adjusted after several computations to include the stress singularity area at the crack tip. The J-integral (and consequently G_C) was calculated at the surface formed by the circular crack front. The thickness of the adhesive layer was set at 0.4 mm, in conformity with the design of the MMB specimen shown in Fig. 2a. The detail of the mesh at the crack tip is given in Fig. 8c. Compared to the previous two studies of Stamoulis et al. [8, 24], an additional parameter was studied here: the initial inclination of the loading arm. This was measured experimentally between 2 to 3° for all MMB

tests that were performed for the needs of the current study. Fig. 8b shows how the loading arm was tilted in the numerical model. It was found that the 2 to 3 degrees initial inclination of the loading arm had no significant influence on the results of G_C calculated here for the adhesive under investigation, at all mode ratios that were examined.

The force value experienced at the peak of each experimental curve was applied to the loading point ('RP-6', Fig. 8a). This point is just after the crack initiation phase [24]; this means that, at this instant of the MMB test, the fracture process zone is well installed ahead of the crack tip and the crack starts to propagate. Therefore, the values for G_C calculated at the peak load are steady-state propagation values; hence, fitting these results with those for G_{IC} calculated by the ISO 25217:2009 standard [4] for the case of the TDCB test is coherent. The boundary conditions were respectively *pinned* and *encastre* for points 'RP-5' and 'RP-7' (*pinned* in Abaqus™means that all translational degrees of freedom are constrained and *encastre* that all translational and rotational degrees of freedom are constrained). The crack length was then adjusted using an optimization algorithm (Nelder-Mead simplex optimization algorithm [31, 32], implemented in Matlab™), until the displacement calculated at the loading point 'RP-6' matched the corresponding experimental value. The adjustment of the crack length to match the experimentally measured force or displacement value (depends if the simulation is performed under displacement or load control respectively) at the peak of the MMB force-displacement curve to calculate G_C, has already been proposed in the past by Stamoulis et al. in [8, 24]. It consists of an alternative technique to bypass the need to experimentally measure the crack length. This is very difficult to realize with good accuracy due to the large micro-fibrillation zone formed ahead of the crack tip, which is generally attributed to the viscosity of structural adhesives. The method was found to work well provided that the elastic mechanical properties of the materials involved are well-known or have been accurately measured. Here, as it was also noted above, the elastic mechanical properties of the substrates used for the simulation were those provided by the supplier (Table 1), and for the adhesive those measured by means of Arcan tests at 0° and 90° (Table 2). The process was repeated for all the experimental curves (Figs. 7a to 7d), in order to build the fracture envelope of the adhesive. The numerical values of the calculated G_C are available in Table 5.

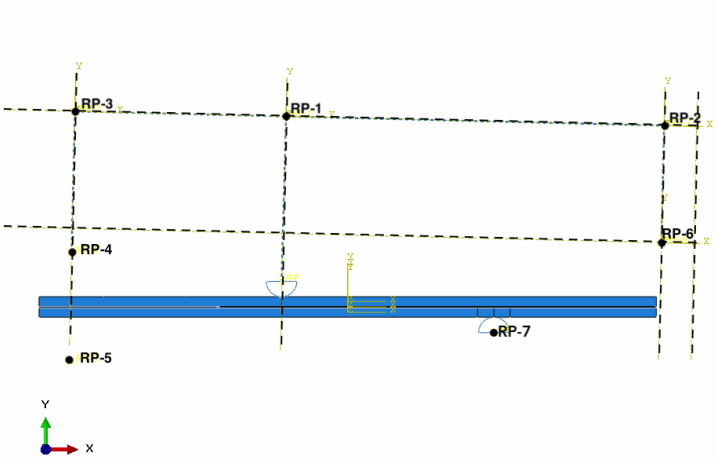

(a) MMB model layout

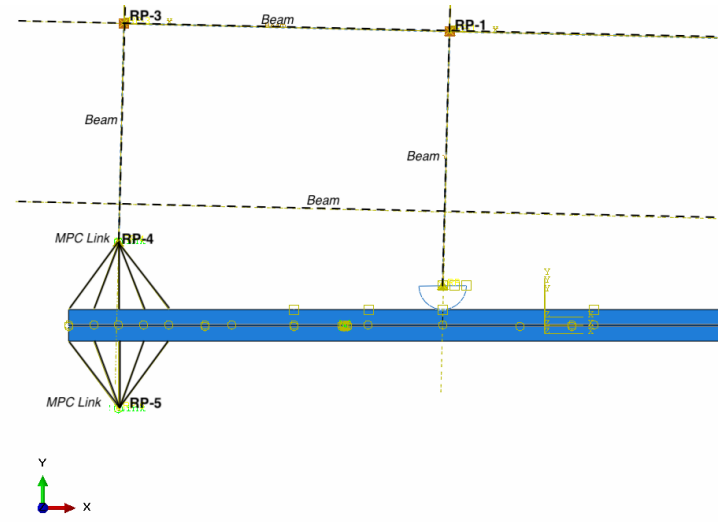

(b) Contacts and interactions modeling

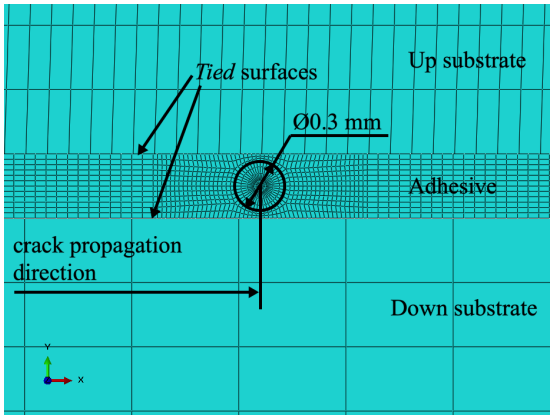

(c) Crack tip meshing

Figure 8: MMB Finite Element model, based on [8]

Specimen ID	Mode ratio [-]	G_C [kJ/m^2]
MMB_20_1	0.2	1.74
MMB_20_2	0.2	1.58
MMB_20_3	0.2	1.72
MMB_40_1	0.4	2.25
MMB_40_2	0.4	2.12
MMB_40_3	0.4	2.61
MMB_60_1	0.6	3.51
MMB_60_2	0.6	3.86
MMB_60_3	0.6	3.79
MMB_80_1	0.8	5.88
MMB_80_2	0.8	5.02
MMB_80_3	0.8	5.39

Table 5: Critical strain energy release rate (G_C) obtained through MMB experiments

2.3.3 Fracture envelope at room temperature (23°C)

The fracture envelope of the adhesive under investigation in the mixed-mode $I + II$ plane as calculated via the TDCB-MMB tests is given in Fig. 9. The trend of the experimental results suggests that a Gong-Benzeggagh (GB) criterion [33, 34] could be suitable for the description of the evolution of G_C with respect to $\frac{G_{II}}{G}$. In the mixed-mode $I+II$ plane, this criterion is mathematically expressed as

$$G_C = G_{IC} + (G_{IIC} - G_{IC}) \left(\frac{G_{II}}{G} \right)^m \tag{4}$$

where m is a dimensionless material parameter to be optimized. The fitting was performed using Matlab™, and the values of the relevant parameters for the GB expression were calculated at: $G_{IC} = 1.57$ kJ/m^2, $G_{IIC} = 7.97$ kJ/m^2 and $m = 1.99$. As a consequence, it was possible to extrapolate a numerical value for G_{IIC}, which is not directly accessible with the MMB test. A significant increase of G_C can be observed with the mode ratio (especially for $\frac{G_{II}}{G} > 0.4$), which has already been evidenced for other structural adhesives showing important ductile behaviour [8, 24, 35]. The numerical values (with two significant digits) used to plot the data in Fig. 9 are provided in Tables 4 and 5.

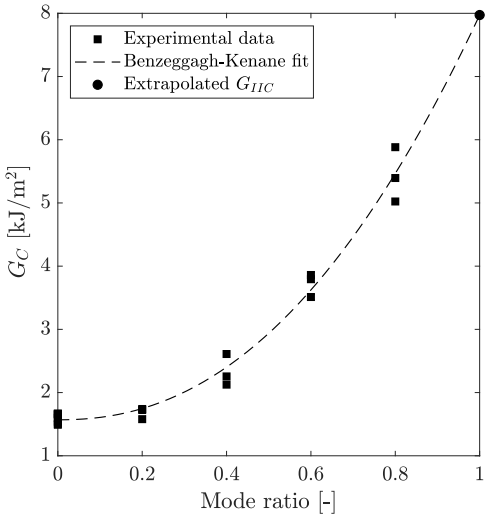

Figure 9: Fracture envelope of the adhesive under investigation at room temperature (23°C).

3 Part II: Investigation of the influence of the temperature using the modified Arcan fixture

As it has already been discussed in the Introduction section, the TDCB and MMB specimen and experimental fixture respectively were unable to fit in the oven used here to perform the tests under temperature, due to their large dimensions. Therefore, for the continuity of this research, the modified Arcan fixture [22] was selected, as it is more compact and could be easily accommodated in the oven used in the present study. This device was shown in the past able to produce equivalent results with the TDCB-MMB tests for the case of structural adhesives [23]. It has already been used by other research teams to examine the fracture properties under mixed-mode $I + II$ loadings for a variety of materials, such as metal alloys [36–39] and composites [40]. It presents several advantages compared to the conventional TDCB-MMB fracture tests, such as: i) the risk of substrate plasticization is fairly limited (the reasons for this phenomenon will be explained in §3.3.1 for the adhesive under investigation here), ii) only one specimen geometry and mounting device are required to complete a full study of the fracture envelope and iii) it also allows to examine the effect compression-shear on crack propagation (this last point is a perspective to the work presented here). In the following sections, specially designed Arcan samples were tested for three loading directions (Fig. 10): pure tensile ($\gamma = 0°$), equally distributed tensile-shear, ($\gamma = 45°$) and pure shear ($\gamma = 90°$). The corresponding mode ratios $\frac{G_{II}}{G}$ were assumed to be equal to 0, 0.5 and 1 respectively; each mode ratio was checked at three different temperatures: 23, 45 and -15°C. The tests at ambient temperature (23°C) with the modified Arcan fixture were needed in order to ensure equivalence of the results with those issued from the TDCB-MMB tests for the adhesive under investigation. This matter was considered important by the authors, since it has only been demonstrated once for the Sikapower®-498 adhesive in [23]. The study continued after this first validation, and the results are presented in the next sections of the manuscript.

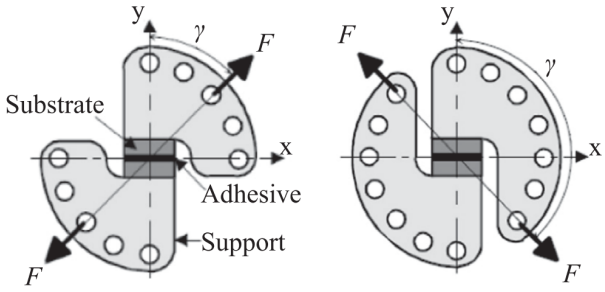

Figure 10: Arcan and modified Arcan loading devices with installed sample and definition of the loading angle γ [22].

3.1 Preparation of the specimens

The Arcan specimen geometry and experimental setup used in this campaign were based on the previously published study by Stamoulis et al. in [23]. The geometry of the samples differs from the typical one used in the past to examine the behaviour of structural adhesives [12, 22, 41, 42]. An overview of the substrates dimensions used for the needs of the present research is given in Fig. 11a. As it can be observed, the bonding surface has a varying cross section: larger at the middle and thinner at the two extremities. This alteration is required to stabilize crack propagation, since two pre-cracks of 6 mm of length were created at the two extremities of each sample. The two pre-cracks were needed to obtain a symmetric sample with regards to the load-line. The substrates were made of Aluminium 2017A (see also Table 1), similarly to the TDCB substrates. The bonding setup is given in Fig. 11b. The thickness of the joint was set at 0.4 mm, in conformity with the TDCB-MMB specimens, by means of calibrated metal sheets. First, the two substrates were brought face-to-face with the metal sheet in-between them. One metallic ring was placed on each substrate (thus two in total); the two metallic rings were screwed together by means of the two top screws (at this stage the four front screws were left loose). The substrates with the metallic sheet and the pre-assembled metal rings were clamped together to set the thickness (Fig. 11c). Next, the metallic rings were fastened on each substrate by means of the four front screws. The system was then unclamped, and the substrates with the metallic rings fixed on them were disassembled by unscrewing the two top screws to remove the metal sheet (Fig. 11d). The adhesive was then applied on the two surfaces to bonded, and the two pre-cracks of 6 mm of length were created by placing two 50 μm thick non-adherent polypropylene films on each side of one of the two substrates at the correct distance. Following this operation, the substrates with the fixed metallic rings were re-assembled via the two top screws. Afterwards, the samples were placed in the Memmert UF110+™ thermal chamber for curing. All screwing procedures described above were performed by means of a torque wrench, in order to avoid possible misalignments and obtain a uniform thickness for the adhesive layer. The bonding process in terms of surface preparation and curing was identical to the one presented before in §2.1 for the TDCB-MMB specimens. Finally, the metallic rings were removed and any excess of the adhesive at the specimen sides was cleaned by grinding with 180 grit sandpaper. The last procedure was needed to facilitate the detection of crack propagation and the measuring of the displacement field on the front

face of each specimen; the latter is required to calculate G_C by applying the methodology that will be presented in §3.3.

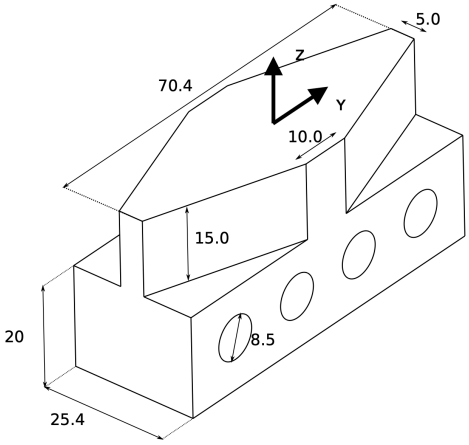

(a) Fracture Arcan substrate design (lengths in mm)

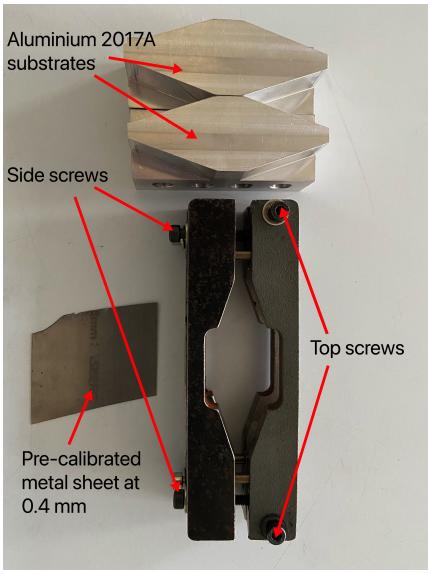

(b) Overview of the bonding setup

(c) Specimen clamping at maximum

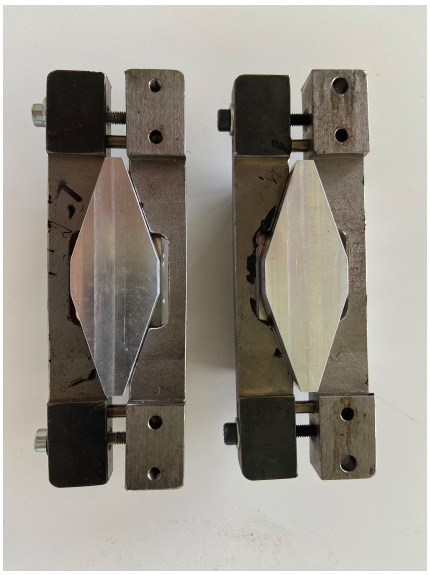

(d) Substrates ready to be bonded

Figure 11: Arcan specimen dimensions and bonding procedure.

3.2 Experimental procedure

Fig. 12 shows the Arcan experimental setup that was used for the needs of the present research. Two identical half-moon pieces were machined to realize the tests. The speckled pattern applied on the surface of each specimen was needed in order to measure the relative displacement between the two substrates by means of the image correlation technique with the GOM™ system. The two horizontal black lines indicate the closest distance from the adhesive layer where this measurement was taken (at around 4 mm from the center of every sample). Each sample was bolted in the Arcan device through the four

upper and the four lower holes. To avoid any relative movements, a plate was fastened on the upper and lower surfaces of the specimen to create a plane contact; the six upper and lower screws (three at the front and three at the back sides of each half-moon piece, as shown in the figure) were used for this purpose. The experiments were realized by means of a universal hydraulic tension-compression machine (Instron™ 1342). The connection of the Arcan fixture with the Instron™ machine was done with the specially designed shafts, also illustrated in Fig. 12. These shafts have a spherical form at the contact point with the Arcan half-moon pieces, in order to avoid transferring any torques during the tests that could alter the results. Each sample was first installed and fixed in the Arcan device as described above, then the whole system (Arcan+sample) was connected with the machine (via the special shafts) at the desired loading angle. As it can be seen in the figure, for the case of the Arcan device used for the needs of the present research, the loading angles can vary from 0° (pure tension) to 135° (compression-shear) with a step of 22.5°. However, as it was also mentioned in the introduction of 3, only the 0° to 90° (pure shear) were examined in this work.

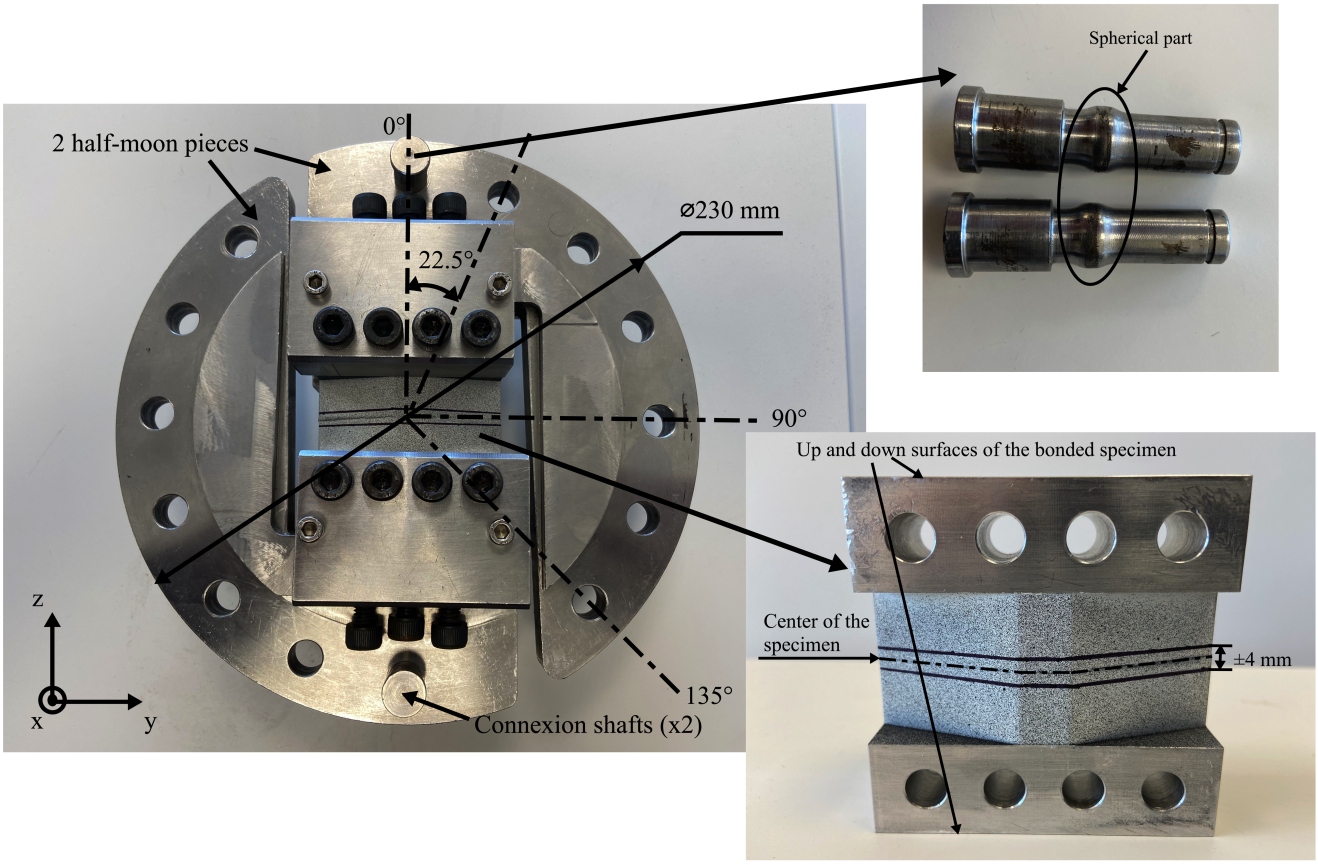

Figure 12: Arcan device used for the needs of the present research

A general aspect of the instrumentation implemented to realize the Arcan experiments for the needs of the present study is given in Fig. 13. The Arcan fixture was surrounded by an adequate thermal enclosure (Servathin™) to perform the tests under temperature. This thermal chamber is equipped with an appropriate view-glass to allow Digital Image Correlation (DIC) measurements at different temperatures. This special view-glass is thermally regulated so as to avoid the formation of any vapor or ice that could

disturb the DIC measurements. In addition, due to the fairly small range of temperatures examined in the present study (-15 to 45°C), no significant ice sticking and/or water drops on the specimen surface were observed. Indeed, no matter the testing temperature, the region of interest in each registered by the GOM™ system cameras images was as clear as the one shown later on in Fig. 18. The images were acquired at 1 Hz frequency. All specimens were tested under displacement control at 0.4 mm/min until complete failure. The exact experimental protocol is given in Table 6. Two samples were considered for each loading case. Therefore, with 3 investigated mode ratios at 3 temperatures, a total of 18 tests were performed. At -15 and 45°C the samples were first conditioned at the desired temperature for one hour before the execution of the experiment. This waiting time was necessary to homogenize the temperature through the specimen volume; it was checked using a dummy sample bonded with the same adhesive, including a thermal probe.

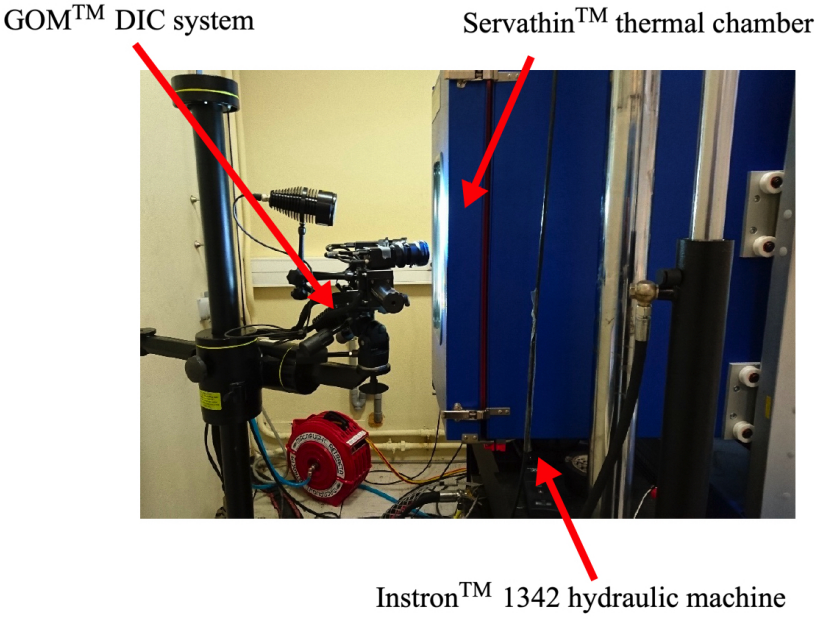

Figure 13: Instrumentation implemented to perform the Arcan fracture tests for the needs of the present research.

Temperature [°C]	γ values [°]	Corresponding mode ratios [-]
-15	0, 45, 90	0, 0.5, 1
23	0, 45, 90	0, 0.5, 1
45	0, 45, 90	0, 0.5, 1

Table 6: Outline of the fracture Arcan tests campaign

3.3 Results, Analysis and Discussions

3.3.1 Validation of the method to measure G_C in the mixed mode I+II plane at room temperature (23°C)

Fig. 14a shows representative load-displacement curves obtained for the Arcan tests performed at room temperature (23°C). On the ordinates axis, the signal from the load sensor of the Instron™ 1342 machine is plotted; as abscissa, the average displacement between the two substrates close to the adhesive layer is used. The latter corresponds to the mean value of the relative displacement between the up and down sections of the two substrates at ± 4 mm from the centerline of each specimen, as measured by means of the GOM™ system (see Fig. 12). An example in the normal (z-axis) direction as a function of the position along the length (y-axis) of a sample tested under pure tension is given in Fig. 14b for three different load levels. The utility of the graphs in Fig. 14 to calculate G_C will be explained below in this paragraph of the manuscript. Concerning the tests performed for $\gamma = 45°$, two load-displacement curves were extracted, by using respectively the normal and tangential relative displacements. As it can be concluded from the results in Fig. 14a, the adhesive showed non-linear mechanical behaviour at all loading angles. In particular, two quasi-linear regimes at different slopes can be distinguished in the curves of Fig. 14a, separated by a yield area. This behaviour was far more pronounced as moving towards the 90° loading angle. This is because the tangential displacement at rupture was more important compared to the normal displacement. The response described above is typical for epoxy adhesives; it has been explained and modeled in the past (*e.g.* in [12]). Concerning the adhesive examined in the present research, it can be remarked that the force at rupture dropped considerably from slightly below 40 kN (at 0°) to slightly above 30 kN at all other loading angles. The fracture surfaces of the Arcan specimens that were tested at room temperature were found all cohesive. An example is given in Fig. 15 for a sample tested at 0°. It should also be noted that the dimensions of the Arcan substrates were visually inspected by means of a Nikon™ V-12 profile projector. It was found that, for the same substrates, their dimensions did not differ significantly before and after the tests from those of the initial design given in Fig. 11a. Therefore, it was concluded that no plastic deformation of the substrates occurred during the Arcan tests that were realized for the needs of the present research, and this for all loading angles γ that were examined. This was expected according to the important size of the Arcan substrates, and in particular to the high values of their width and height (at 25.4 and 35 mm respectively, Fig. 11a). An other reason could be that the whole joint is loaded in the case of Arcan tests, as opposed to classical fracture mechanics tests, for which only a restricted part of the adhesive at the vicinity of the crack tip is loaded.

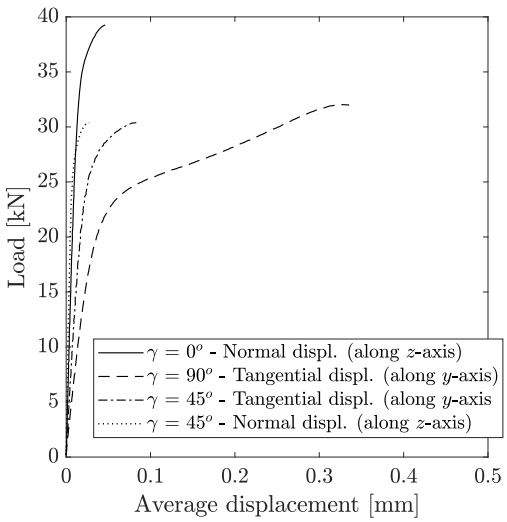

(a) Load-displacement mean curves for Arcan fracture tests

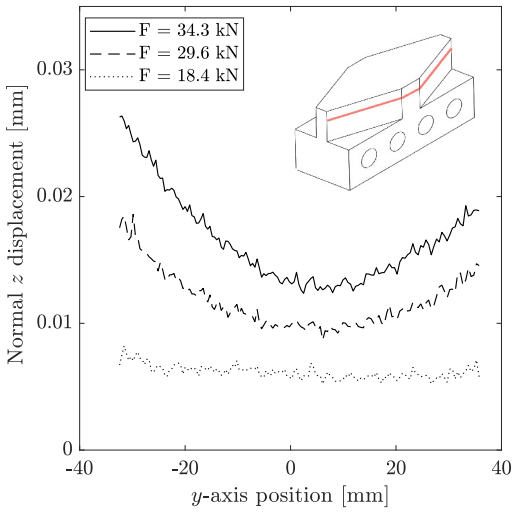

(b) Normal displacement along the edge (in red) of one of the two samples tested under tension ($\gamma = 0°$) at three load levels

Figure 14: Arcan experimental results (23°C), z & y denote the normal and tangential displacements with respect to the adhesive layer.

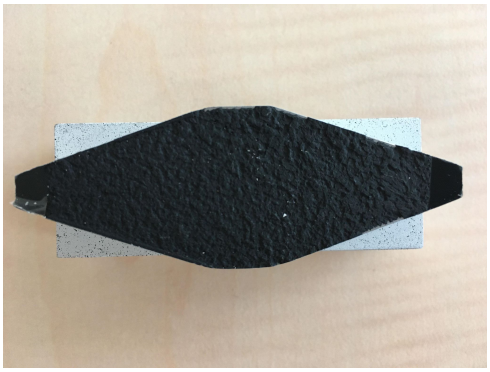

Figure 15: Exemple of a face of rupture ($\gamma = 0°$, 23°C). The marks of the pre-cracks on the left and right sides of the sample can be clearly distinguished.

Based on the previous observations concerning the absence of plastic deformation of the substrates and in order to be in conformity with the TDCB-MMB tests, it was decided to analyze the experimental results issued with the Arcan fixture under the linear elastic assumption to calculate G_C. The method used here was based on the previously published work by Stamoulis et al. [23]. In particular, following the form of the curves in Fig. 14a, it was supposed that any loss of the initial stiffness was due to crack initiation and propagation rather than to the plastification of the joint. This assumption is coherent at the beginning of the yield area and until the influence of plasticity of the adhesive on the fracture results is not very significant. Thus, the identification of the point to perform the computation for G_C is very crucial. In the previous publication, this point was identified for the specimens tested at 0° and 45° as

the last point where the crack was visually inspected to propagate inside the adhesive layer. At this moment, the relative displacement between the two substrates was applied as input in a finite element model of the test, and the numerical crack length at both sides of the specimen was manually optimized so that the reaction force matched the experimentally measured force value. G_C was then calculated by means of the domain contour integral method for the numerically adjusted value of the crack length. Concerning the 90°, no crack propagation has been observed for the Sikapower®-498 adhesive in [23]; thus, the computation for G_{IIC} was realized at the point just before the apparition of the shear bands (see also [43]) by simply applying the initial crack length value of 6 mm. This type of analysis gave slightly higher values for G_C compared to those calculated by the conventional TDCB-MMB tests at the pure I & II modes, and almost the same for $\gamma = 45°$. The differences for the pure I & II modes were mainly been attributed to the influence of the plasticity of the joint on the fracture results. An exemple for crack propagation under mode I as published by Stamoulis et al. [23] is given in Fig. 16.

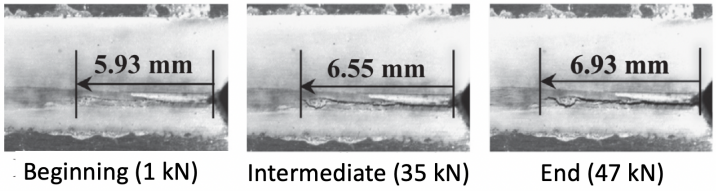

Figure 16: Stable crack propagation evidenced for Arcan fracture tests [23]

.

The behaviour of the adhesive under investigation here when tested with the Arcan fixture to study its fracture properties, was similar to the one described just above for the Sikapower®-498 adhesive. Hence, at it was also done in [23], the calculation of G_C was realized numerically by means of the domain contour integral method. This is also because, to the authors knowledge, no analytical formulas to extract G_C from Arcan-based tests exist until the time of publication of the present article. The model is presented in Fig. 17; it was built in 3D, because of the varying bonding section of the substrates (Fig. 11a). In order to simplify matters and gain in computational time, the crack propagation was considered symmetrical at both sides of each specimen. The relevance of this hypothesis will be discussed later on in the manuscript; it could not be applied in [23] because of the larger bonding surface that has been used in that work. Therefore, in the present study, 1/8th of the complete sample was simulated, using the following symmetry planes with respect to the center of the adhesive layer (Fig. 17c): i) $(\vec{x}, \vec{z})$, same crack propagation on the right and left side of the specimen, ii) $(\vec{x}, \vec{y})$, the crack propagates in the middle of the adhesive layer and iii) $(\vec{y}, \vec{z})$, same crack propagation on the front and back sides of the specimen. It is obvious that the last symmetry plane implies also that the displacement field measured at the surface of the specimen (see Figs. 12 and 18) was the same through its width; this should be all right based on the nature of the Arcan device to load samples similarly along the out-of-loading plane axis [43] (x-axis in Fig. 17). According to all previous remarks, half of the adhesive layer was modeled (0.2 mm, Fig. 17b) and the substrate material was extended until 4 mm from the bottom (Figs. 12 and 17a). The geometry was meshed using 8-node linear brick elements (C3D8, [30]); their dimensions were set after having performed a preliminary

mesh convergence study. The non-homogenous mesh between the adhesive layer and the substrates is well noticed in Fig. 17b. This was done to gain in computational time, similarly to the choice that was made for the modeling of the MMB test in §2.3.2. At the up border of the adhesive layer, the option *tie* of Abaqus™ was used to simulate the adherence with the substrate. The detail of the crack tip given in Fig. 17b was taken from the front face of the numerical model shown in Fig. 17a. A cylindrical domain of Ø0.3 mm was created for the crack front in order to calculate the J-integral.

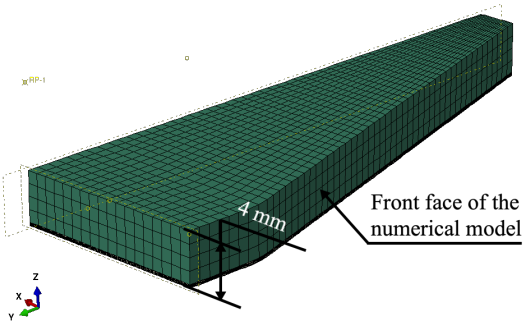

(a) Arcan FE model ($1/8^{th}$ of the complete sample)

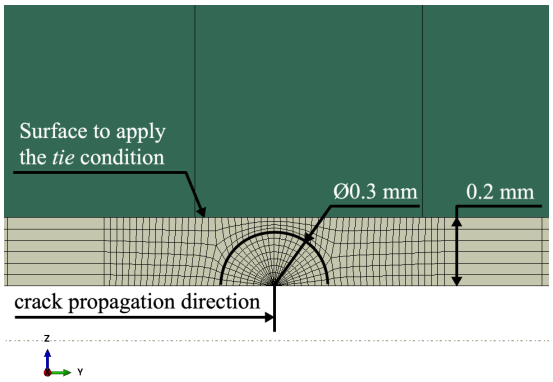

(b) Crack tip mesh (dark green: adherend - light green: adhesive)

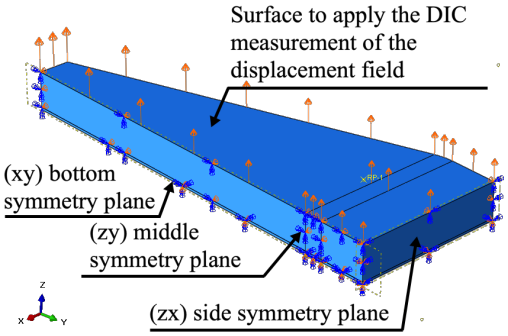

(c) Boundary conditions applied to the model

Figure 17: Arcan Finite Element model

Fig. 18 shows the DIC surfaces measured at the front face of every Arcan sample by means of the GOM™ system. In particular, two regions of interest (R_1 and R_2) were considered on the up and down substrates respectively, both being at a minimal distance of ±4 mm from the centerline of each specimen (see also Fig.12). Their exact location is schematized in Fig. 18c too, where it can be remarked that their height was taken equal to 10 mm. The DIC measurements were processed to calculate the relative displacement of the two substrates at the vicinity of the adhesive layer. At all loading angles and temperatures, the displacements u in the regions R_1 and R_2 were calculated for each facet and averaged over the whole regions as follows

$$
\begin{aligned}
u^{\vec{z}}_{R_i} &= \overline{u(y,z)}^{\vec{z}} \text{ with } [y,z] \in R_i \\
u^{\vec{y}}_{R_i} &= \overline{u(y,z)}^{\vec{y}} \text{ with } [y,z] \in R_i
\end{aligned}
\tag{5}
$$

Afterwards, if $\Delta u^{\vec{z}}$ & $\Delta u^{\vec{y}}$ denote the relative displacement between the two substrates along the normal z and the tangential y to the adhesive layer axis respectively, the following equations were applied

$$
\begin{aligned}
\Delta u^{\vec{z}} &= u^{\vec{z}}_{R_1} - u^{\vec{z}}_{R_2} \\
\Delta u^{\vec{y}} &= u^{\vec{y}}_{R_1} - u^{\vec{y}}_{R_2}
\end{aligned}
\tag{6}
$$

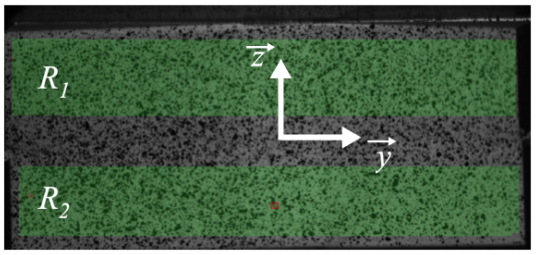

(a) Regions of interest R_1 and R_2

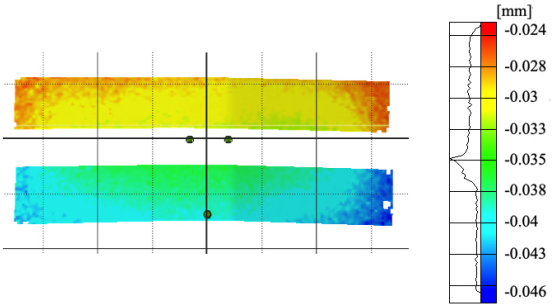

(b) Normal displacements field computed by means of digital image correlation

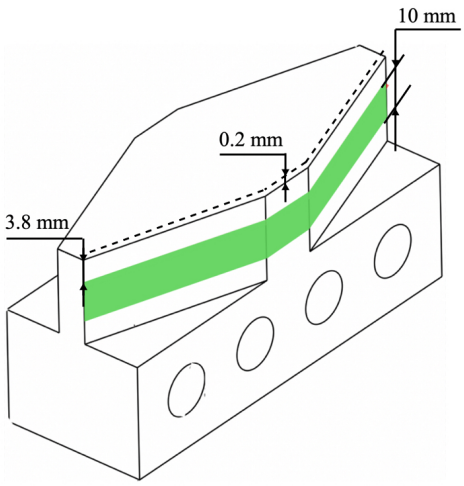

(c) Location of the surface of interest on the front faces of an Arcan substrate

Figure 18: DIC measurements performed on an Arcan fracture sample.

The displacements $\Delta u^{\vec{z}}$ & $\Delta u^{\vec{y}}$ computed by DIC were only used to load the up surface of the substrate in the numerical model (Fig. 17c), at the appropriate force level of the load-displacement curves. This loading technique implies that the sample is homogeneously loaded along its width (x-axis, Fig. 17c), as it was also discussed above. The identification of the appropriate force level to perform the previously

described operation will be discussed below. Fig. 14b illustrates the trend followed by these displacements for three loads during one of the two tensile tests at room temperature. The graph shows that in the beginning the adhesive strains uniformly along its length (that is along the y-axis). As long as the test continues, the sides of the adhesive start to deform more than the center. Finally, one side of the adhesive deforms more compared to the other one and the sample breaks. These observations can be explained by the opening of the crack lips, which become more and more important while the test continues along the tensile direction (at $\gamma = 0°$ & $45°$). On the other hand, no significant difference of the displacement values along the y-axis until rupture was measured between the two sides of the adhesive for the tangential displacements (at $\gamma = 45°$ & $90°$). This behaviour described above is similar to the one observed for the Sikapower®-498 adhesive in [23]. It means that crack initiation and propagation takes place under tension, at least for the side of the specimen which strains more. On the contrary, no crack propagation could be attributed to shear loading for the Arcan experimental methodology as it was set here. It is easily noticed that the symmetry hypothesis expressed earlier along the $(\vec{x}, \vec{z})$ plane (Fig. 17c) is relevant for the case of the transverse displacement. For the case of the normal displacement, this symmetry is coherent until a certain force level (maximum 35 kN for the specimen shown in Fig. 14b); at higher force levels, the slight shift (or tilt) that was observed suggests that the two cracks pre-formed at each end of the sample do not propagate at the same rate. This phenomenon was most likely due to inhomogeneities in the adhesive material and/or to experimental errors that could not be avoided (*e.g.* creation of equally lengthened pre-cracks at the extremities of the joint etc.). Nonetheless, the computation for G_C was not performed in the end of the test but in an intermediate point (the identification of which will be presented below). Since the difference between the amplitude of the normal displacement between the two sides of the specimen at that point was not found significant, it can be considered that the symmetry hypothesis along the $(\vec{x}, \vec{z})$ plane (Fig. 17c) is coherent for the normal direction too.

Based on the previous discussions, a methodology was put into use to compute G_C at the different load ratios applied on the adhesive by means of the Arcan device. Compared to the method previously published by Stamoulis et al. in [23], two major improvements are proposed here: i) an automated procedure to calculate G_C and ii) a more appropriate manner to identify the load level to realize this calculation. Concerning the former point, a script was programmed in Matlab™ to avoid the manual computations that were performed in [23]. For the case of normal load ($\gamma = 0°$ & $45°$), the script permitted to optimize the numerical crack length (Fig. 17b) until the reaction force matched the 1/8th of the experimentally measured one. This optimisation was realized using the same algorithm as for the MMB tests analysis ([31, 32]); the error function ε to minimize is expressed by the following equation

$$\varepsilon = \sqrt{\left[F_R(\Delta u^{\vec{z}}, a) - F_{exp}(t)\right]^2} \tag{7}$$

where $F_R(\Delta u^{\vec{z}}, a)$ is the FE reaction force for a given imposed normal displacement field $\Delta u^{\vec{z}}$ and a given numerical crack length a, and $F_{exp}(t)$ is 1/8th of the experimental load at a given instant t of the test, corresponding to the instant where the displacement field $\Delta u^{\vec{z}}$ was maintained. Concerning the shear load, two cases were considered depending on the test: i) at $\gamma = 45°$, the computation of G_{II} (the strain

energy release rate under mode II) was performed using the optimized numerical crack length a issued from the calculations realized for the normal portion of the load by means of the methodology described above; ii) at $\gamma = 90°$ the displacement field $\Delta u^{\vec{y}}$ maintained at a certain force level was directly applied to calculate G_{IIC} by using the initial crack length value of 6 mm. For both previous cases, no cross-check between the numerical and experimental values of the force was made. These choices were set following the experimental observations described earlier that no crack propagation could be attributed to shear load here; this has also been witnessed in [23]. Fig. 19 illustrates the flow chart of the methodology that was created in the present study to analyze the Arcan tests and compute G_C at different load ratios.

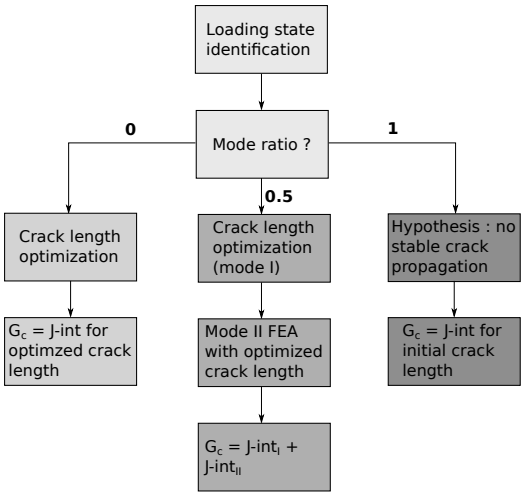

Figure 19: Suggested methodology to analyze the Arcan tests and compute G_C at different load ratios.

The identification of the load level to perform the calculation for G_C via the data coming from Arcan tests is very crucial, for the reasons discussed earlier in this paragraph. The visual method used in [23] requires very accurate optical equipment and is very difficult to implement. In order to compensate for these drawbacks, an alternative procedure is proposed here based on a direct analysis of the force-displacement experimental data. Basically, two indications about the loading level to choose for the G_C calculation were considered: i) it should be high enough for the crack to propagate; ii) it should be low enough to ensure coherent application of the LEFM assumption, given the non-linear behaviour experienced by the adhesive under investigation during the Arcan tests (Fig. 14a). Due to the fairly vague implications of these conditions, the J-integral (Eq. (3)) was computed for a whole set of loading states under the linear elastic hypothesis for the adhesive and the substrates, for the experiments performed at ambient temperature (23°C). The values of the J-integral as a function of the applied load calculated for one of the two tests performed under tension (0°) and one of the two tests performed under shear (90°) are given Figs. 20a to 20b respectively. In the figure legends, the J-integral is referred to as strain energy release rate, which is correct since the simulations where realized under linear elasticity. Both graphs show that the evolution of the J-integral can be defined by two domains and a transition zone in-between. Moreover, as expected, the values of the J-integral explose to non-realistic ones after the

transition area, while moving towards the end of the test. This phenomenon can be explained by the influence of the plasticity of the adhesive layer on the fracture results, which was not considered for these computations. Comparing the curves of Figs. 20a to 20b with the corresponding load-displacement curves (Figs. 20c to 20d), it can be remarked that the two domains of the J-integral correspond to the two distinct quasi-linear zones of the experimental curves and the transition zone to the yield area. It is obvious that the J-integral evolutes similarly along the tensile and shear directions, when looking at the load-displacement curves plotted for one of the two tests performed at $\gamma = 45°$ in Figs. 20e to 20f.

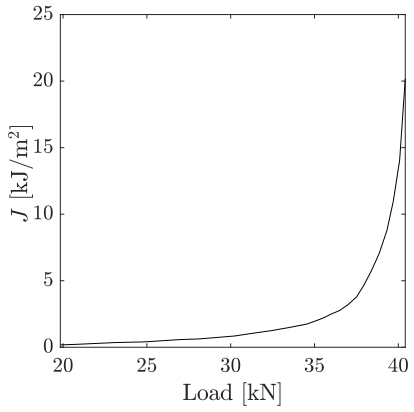

(a) Strain energy release rate versus applied load (tensile Arcan fracture test)

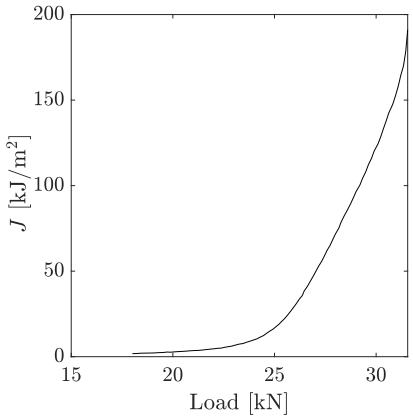

(b) Strain energy release rate versus applied load (shear Arcan fracture test)

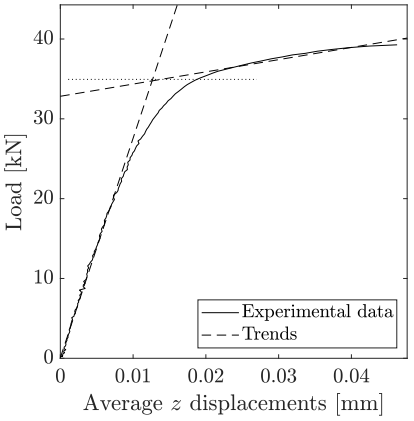

(c) G_C calculation point definition (dotted line, tensile Arcan fracture test)

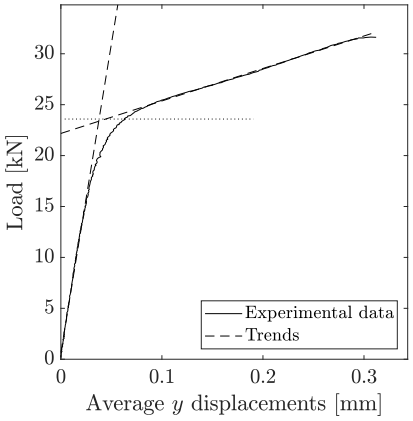

(d) G_C calculation point definition (dotted line, shear Arcan fracture test)

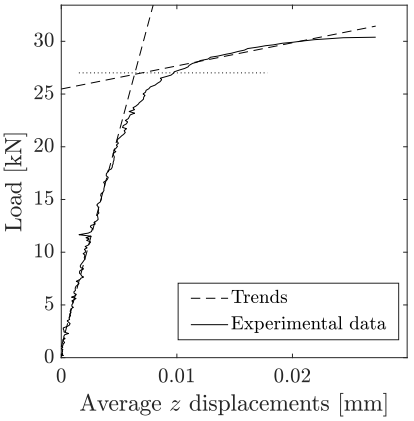

(e) G_C calculation point definition (dotted line, tensile-shear Arcan fracture test, normal displacements)

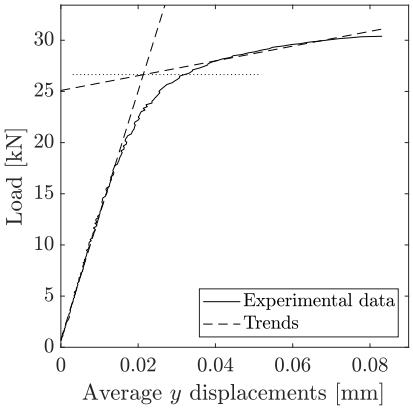

(f) G_C calculation point definition (dotted line, tensile-shear Arcan fracture test, tangential displacements)

Figure 20: Strain energy release rate as a function of the applied load and determination of the experimental point to use for the computation of G_C.

In order to locate the instant to calculate G_C on the Arcan load-displacement experimental curves registered for the needs of the present research, an empirical criterion was established here. This was required to bypass the need to use the visual equipment implemented in [23] as discussed also above, which was impossible to adapt here due to the thermal chamber enclosing the Arcan device for the tests under temperature (Fig. 13). The method will be illustrated for one test chosen at random among the two performed for each one of the $\gamma = 0°$, $45°$ and $90°$ loading angles (Figs. 20c to 20f). For $\gamma = 45°$, two datasets were always available: a first one relative to the normal displacement (Fig. 20e) and a second one relative to the tangential displacement (Fig. 20f). For all curves, the two quasi-linear zones described earlier in this paragraph of the manuscript can be distinguished. These zones will be referred here as "elastic" and "plastic" domains. To compute them, the evolution of the stiffness of each sample along with the progression of the test was monitored as follows: i) the elastic domain was defined starting from the beginning of the test and until the stiffness decreased by 10%; ii) the plastic domain was defined starting from the end of the test and until the stiffness increased by 10%. Since the trends of the load-displacement curves inside these two domains were assumed quasi-linear, the data were fitted by 1^{st} order polynomials for every specimen, as shown in the figures. G_C was then calculated at the load level corresponding to the intersection point between the previous two polynomials, by loading the FE element model (Fig. 17) with the relative displacement field between the two substrates measured along the length of the specimen (Fig. 14b,Fig. 18 & Eq. (6)) at that instant. Concerning the experiments shown in Figs. 20c to 20f, these load levels were calculated at: 34.8 kN for the test at $\gamma = 0°$, 23.4 kN for the test at $\gamma = 90°$ and 26.7 kN for both the normal and tangential directions of the test at $\gamma = 45°$. The values for G_C obtained at room temperature by using the previous empirical criterion along with the proposed FE model for the Arcan fracture tests are given in Table 7. It must be noted here that the terms elastic and plastic employed before were used simply to identify the two quasi-linear domains, and should not in any case be related to the mechanical behaviour of the adhesive during the Arcan fracture tests. Such an analysis would require a very heavy instrumentation and a much more thorough investigation of the experimental results (see also [12]), which is out-of-the-scope of the present paper. Moreover, the characterization of the state of the crack (initiated or propagated) at the point chosen to perform the computation for G_C was not performed in this study; this would be an interesting perspective to the work presented here. For the needs of the present research, the coherence of the empirical criterion that has been implemented was validated by comparing with the TDCB-MMB results, as it will be shown below. Nonetheless, some information regarding crack propagation during the Arcan fracture tests issued from [23], was provided earlier in this paragraph of the manuscript (see also Fig. 16).

Specimen ID	Temperature [°C]	γ [°]	Mode ratio [-]	G_C [kJ/m^2]
AR0_23_1	23	0	0	1.73
AR0_23_2	23	0	0	1.81
AR45_23_1	23	45	0.5	2.83
AR45_23_2	23	45	0.5	2.77
AR90_23_1	23	90	1	8.40
AR90_23_2	23	90	1	8.43

Table 7: G_C values issued from the Arcan tests performed at room temperature for $\gamma = 0°$, 45° and 90°.

Comparing the results issued from the Arcan fixture (Table 7) with the corresponding ones issued from the TDCB-MMB tests (Tables 4 & 5), it can be remarked that the values for G_C computed from both methodologies do not differ significantly. This can be clearly understood when also plotting G_C vs $\frac{G_{II}}{G}$ in Fig. 21a. Taking a closer look on the previous observations, it can be noted that: i) at the pure I & II modes, the Arcan fracture tests yielded slightly higher values for G_C compared to the ones derived from the TDCB-MMB tests; ii) in the mixed mode $I + II$ plane the values of G_C at $\gamma = 45°$ were almost the same compared to those issued after fitting the GB criterion (Eq.4) on the TDCB-MMB measurements of G_C. All these points are in accordance with the conclusions published before in [23] for the Sikapower®-498 adhesive. However, in [8], G_{IC} was measured at around 2.93 kJ/m^2 and G_{IIC} at 11.03 kJ/m^2 with the TDCB-MMB method; on the other hand, in [23], G_{IC} was found between 2.98 & 3.45 kJ/m^2 and G_{IC} between 12.03 & 13.12 kJ/m^2. It is obvious that the differences found here between the TDCB-MMB test results and those of the Arcan device for G_C are lower for the adhesive under investigation. Therefore, it can be concluded that the use of the empirical criterion presented above to identify the instant to perform the computation for G_C together with the FE model of the Arcan test seem to work well and even better than the visual inspection of the test implemented in [23]. Nonetheless, a thorougher analysis of the experimental results issued from Arcan fracture-type tests (such as the ones presented here) is required to validate the procedure proposed in this work (*e.g.* investigation of the state of the crack tip at the loading point identified to perform the computation, influence of the plasticization of the joint on the fracture results etc.). Indicatively, Fig. 21b shows a comparison between the fracture envelopes found from the TDCB-MMB and the Arcan tests, after fitting the GB criterion (Eq.4) for both cases. The following values were identified for the Arcan fracture tests: $G_{IC} = 1.77$ kJ/m^2, $G_{IIC} = 8.41$ kJ/m^2 and $m = 2.69$. As expected, the curves in Fig. 21b are almost superposed.

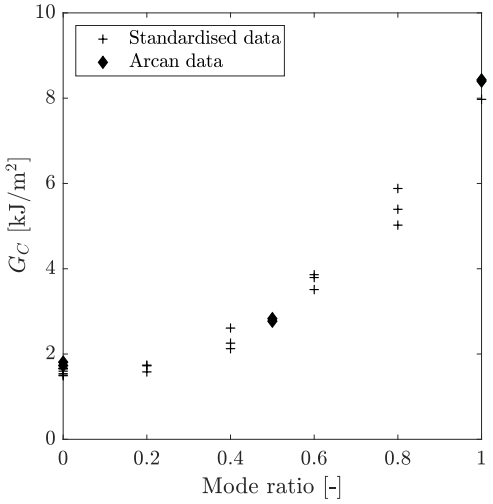

(a) Fracture envelopes of the adhesive at room temperature (comparison between standardized methods and an Arcan-based method)

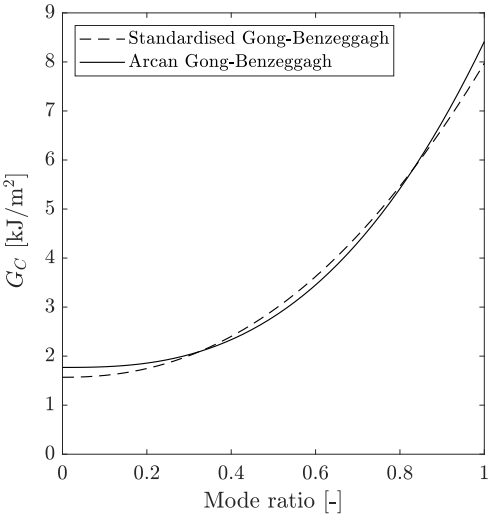

(b) Comparison between the Gong-Benzeggagh criterions fitted to the standardized (TDCB/MMB) data and to the Arcan data

Figure 21: Standardized tests results versus Arcan tests results (at 23°C).

3.3.2 Study at -15°C and 45°C

The method of computation of G_C by means of Arcan tests as described in §3.3.1 was performed also for the other two temperatures (-15°C and 45°C) that were examined for needs of the present research. The values calculated for the adhesive under investigation are given in Table 8. Fig. 22a shows a comparison between all the fracture envelopes that were measured in this work; the trends for G_C as a function of the temperature at $\gamma = 0°$, 45° and 90° are illustrated in Figs. 22b to 22d respectively. All graphs in Fig. 22 witness for the adhesive under investigation that, from -15°C up to 45°C: i) G_C decreased with the increase of temperature and ii) this decrease was quasi-linear for all loading angles γ. In general, an increase in temperature corresponds to a positive energy intake for the heated material(s). Therefore, one could assume the previous results logical, since G_C corresponds to the potential energy released once a crack propagates in a solid medium over a unit area. This is also reinforced by the fact that: i) the force at rupture increased with the decrease of the temperature for the adhesive under investigation and ii) that the Arcan-based force experimental data were processed here under the linear elasticity assumption. However, all these do not mean that all introduced energy due to the increase of the temperature was spent to crack propagation, since other phenomena are also involved (*e.g.* non-linearity of the adhesive material, thermal expansion of the materials, possible phase changes etc.). A similar tendency was obtained for the fracture properties of a structural adhesive submitted to mode I and II loadings in [19] and [20] respectively (as also discussed in the introduction section) when outside the T_g area, in spite of the fairly high scattering of the experimental data. Moreover, in the research performed by Moller et al. in [44], the maximum value for G_{IC} was found at 80°C for a T_g of the studied adhesive equal to 125°C. Still in that study, a slight decrease between 20°C and 50°C was measured for G_{IC}. In the work

presented here, the T_g of the adhesive under investigation was obtained by DSC measurements (Fig. 3b) at around 88°C. Thus, comparing to the findings in [19, 20, 44], the continuous decrease of G_C with the increase of the temperature illustrated in the graphs of Fig. 22 could seem unnatural. Maybe an increase of G_C closer to 88°C might appear, if performing tests at higher temperatures with the adhesive under investigation. Nonetheless, the range of temperatures from -15°C up to 45°C was determined together with the industrial partner of the project and in conjunction with the final application. Yet, performing additional tests at higher and/or lower temperatures would be an interesting perspective, which would also allow for a more detailed comparison with the results reported in [19, 20, 44]. Finally, it should be mentioned that the fracture surfaces of all Arcan specimens tested at -15°C and 45°C were found cohesive, similar to the tests at room temperature presented in §3.3.1.

Specimen ID	Temperature [°C]	γ [°]	Mode ratio [-]	G_C [kJ/m^2]
AR0_m15_1	-15	0	0	3.85
AR0_m15_2	-15	0	0	3.38
AR45_m15_1	-15	45	0.5	4.54
AR45_m15_2	-15	45	0.5	4.43
AR90_m15_1	-15	90	1	10.59
AR90_m15_2	-15	90	1	10.82
AR0_45_1	45	0	0	0.55
AR0_45_2	45	0	0	0.77
AR45_45_1	45	45	0.5	0.96
AR45_45_2	45	45	0.5	1.19
AR90_45_1	45	90	1	4.01
AR90_45_2	45	90	1	4.65

Table 8: G_C values for various γ values at -15°C and 45°C.

At this point, it is interesting to discuss about some important parameters that have not been taken into account here in the analysis of the results for G_C at the three temperatures (-15°C, 23°C and 45°C). When conditioning the samples for 1h before executing the tests at -15°C and 45°C (see §3.2), thermal stresses were generated due to the mismatch of the Coefficient of Thermal Expansion (CTE) between the adhesive and the substrates. In addition, the curing procedure (see §2.1.3) resulted to an initial stress field in the adhesive layer. It is obvious that such time dependent phenomena were not taken into consideration by means of the linear elastic assumption employed in the FE models of the tests that were created for the needs of the present research. Their inclusion in the computations of G_C would require a very thorough characterization of the mechanical behaviour of the adhesive under investigation (*e.g.* examination of the viscoelastic behaviour of the adhesive, its dependence on hydrostatic pressure etc., see also [12]). The consideration of the mechanical behaviour of a structural adhesive in the calculations of G_C at different mode ratios gave interesting results at room temperature in [21]. However, performing a similar work under different temperatures is out-of-the-scope of the present article, as it would make it too long and

too hard to read and follow. It must also be pointed out that so far these aspects have not been examined in the previously published works dealing with the influence of the temperature on the fracture properties of structural adhesives (like in [19, 44]). The aim here was to make a first investigation on the influence of the temperature on the results for G_C of the studied adhesive via a simplified analysis; as such, the LEFM theory was used.

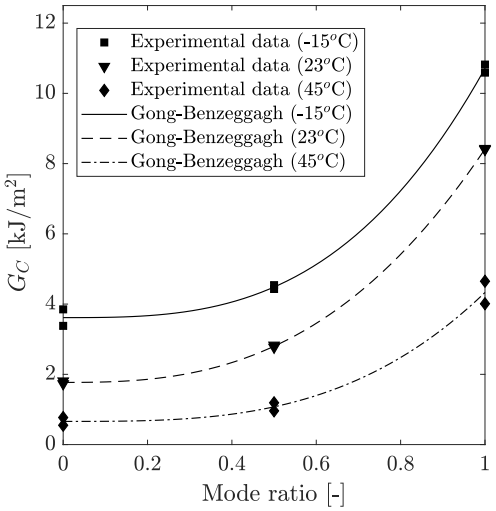

(a) Fracture envelopes computed with means of the Arcan geometry for various temperatures

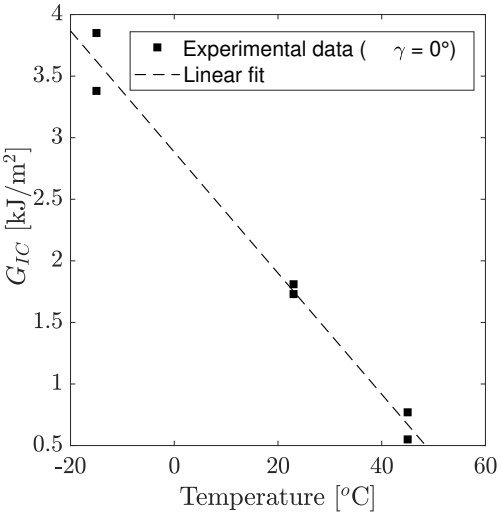

(b) Mode I critical strain energy release rate as a function of the temperature

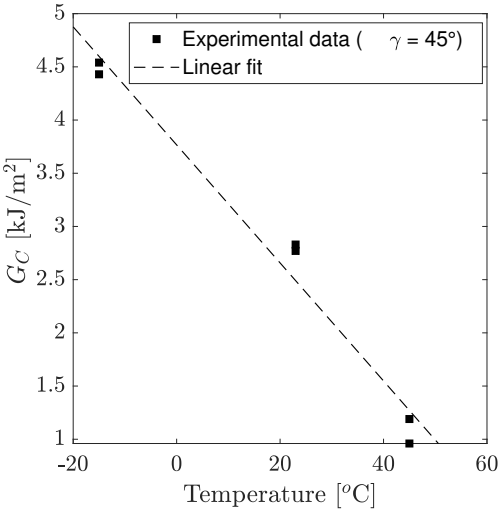

(c) Mixed-mode $I + II$ critical strain energy release rate as a function of the temperature

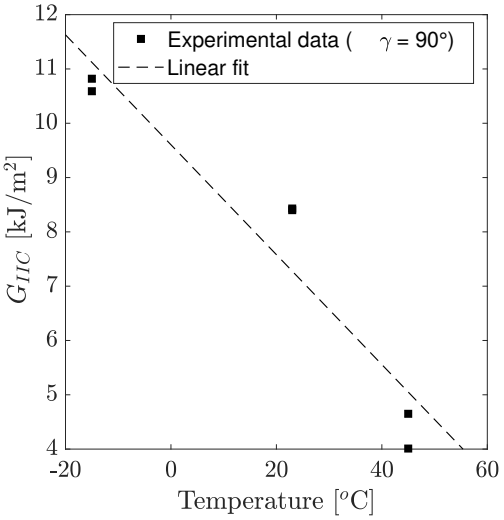

(d) Mode II critical strain energy release rate as a function of the temperature

Figure 22: Fracture properties of the adhesive under investigation at -15°C, 23°C and 45°C

4 Conclusions and Perspectives

In the present study, the fracture properties of a structural adhesive were examined at three temperatures (-15°C, 23°C and 45°C). Due to the limited space of the thermal chamber which was used to realize the tests, it was decided to perform this research by means of the Arcan fixture. However, in order to guarantee the relevance of the results, first the fracture envelope of the adhesive under investigation in the mixed mode $I + II$ plane was identified via conventional TDCB-MMB tests at room temperature (23°C). It was shown that the evolution of G_C as a function of the mode ratio for the studied adhesive can be adequately described by means of the GB criterion [33, 34]. Concerning the Arcan tests, a methodology was created here to calculate G_C for various loading angles, by improving the previously published method by Stamoulis et al. in [23]. First, an appropriate specimen geometry was created in order to allow stabilization of crack propagation. Next, a compact Arcan fixture to be placed in the oven was designed to test the bonded specimens. The procedure proposed in the present study to calculate G_C by means of experiments realized with the Arcan device is composed of four main steps: i) a FE modelling of the test by using only 1/8th of the specimen along with the definition of the appropriate symmetry planes; ii) the identification of the point to perform the computation by establishing an empirical criterion based on a direct evaluation of the force-displacement curves; iii) at this point, application in the FE model of the relative displacement between the two substrates close to the adhesive layer, as measured by the DIC technique; iv) optimization of the numerical crack length to match the experimentally measured force for the normal to the adhesive layer displacements ($\gamma = 0°$& $45°$), or direct computation of the value of the strain energy release rate for the transverse to the adhesive layer direction, either by applying at the identified point the optimized value of the numerical crack length for $\gamma = 45°$ or the initial value of the crack length at 6 mm for $\gamma = 90°$. The results at ambient temperature showed excellent match between the fracture envelopes identified by means of the TDCB-MMB and the Arcan device tests. According to this promising result, the Arcan tests were continued for the other two temperatures of -15°C and 45°C. For the range of temperatures examined, it was found here that the values for G_C decreased with the increase of the temperature.

It is obvious that the results obtained in the present work open a large field of investigation. First, the Arcan based methodology to calculate G_C can still be improved. For instance, the empirical experimental criterion to identify the point to perform the computation for G_C yielded very satisfactory results. However, a deeper analysis of the experimental data is required to validate this procedure, namely by examining the crack state (initiated or propagated) at this specific point. In addition, as it was also discussed in §3.3.2, all experimental measurements here were exploited using a simplified framework by considering the adhesive and the substrates under the linear elasticity assumption. Therefore, it would be interesting to investigate the influence of the mechanical behaviour of the adhesive under investigation on the fracture properties, especially under temperature. Moreover, the inclusion in the FE models presented in this manuscript of the initial stress state developed in the samples due to curing and conditioning, is also expected to impact the results for G_C. Other perspectives include for example the realization of tests at other temperatures inside and/or outside the range that was chosen here; this would provide

interesting information on the evolution of G_C as a function of the temperature, which was supposed linear here due to the low number of experimental points that were obtained. Finally, tests at different relative humidities would also provide interesting information, especially if coupled with a variation of the surrounding thermal environment. Some of these aspects are currently being under investigation, and will make the subject of future publications.

References

[1] A.A. Griffith. "The Phenomena of Rupture and Flow in Solids". In: *Philosophical Transactions of the Royal Society of London* 221 (1921), pp. 163–198.

[2] *ASTM D3433-99,Annual book of ASTM standards*. Standard. Philadelphia, PA: ASTM, 2012.

[3] "BS 7991:2001 - Determination of the mode I adhesive fracture energy, $G_{I,C}$, of structural adhesives using the double cantilever beam (DCB) and tapered double cantilever beam (TDCB) specimens". In: *Adhesives*. 2001.

[4] "ISO 25217:2009 - Determination of the mode 1 adhesive fracture energy of structural adhesive joints using double cantilever beam and tapered double cantilever beam specimens". In: *Mechanical behavior*. Geneva, CH, 2009. Chap. Adhesives.

[5] B R K Blackman et al. "Measuring the mode I adhesive fracture energy, G IC , of structural adhesive joints: the results of an international round-robin". In: *International Journal of Adhesion & Adhesives* 23 (2003), pp. 293–305. DOI: 10.1016/S0143-7496(03)00047-2.

[6] "ASTM D6671/D6671M-13e1". In: *Annual book of ASTM standards*. Philadelphia, PA: ASTM, 2013. Chap. Composites.

[7] "ASTM W.K. 22949". In: *Annual book of ASTM standards*. Philadelphia, PA: ASTM. Chap. Composite.

[8] Georgios Stamoulis et al. "On the experimental mixed-mode failure of adhesively bonded metallic joints". In: *International Journal of Adhesion and Adhesives* 51 (2014), pp. 148–158.

[9] F Ducept, P Davies, and D Gamby. "Mixed mode failure criteria for a glass/epoxy composite and an adhesively bonded composite/composite joint". In: *International Journal of Adhesion & Adhesives* 20 (2000), pp. 233–244.

[10] M. Costa et al. "Static assessment of the mixed-mode behaviour of three epoxy adhesives". In: *Engineering Fracture Mechanics* 182 (2017), pp. 552–565. DOI: 10.1016/j.engfracmech.2017.05.028.

[11] Marcio Moreira Arouche et al. "Strain-based methodology for mixed-mode I+ II fracture: A new partitioning method for bi-material adhesively bonded joints". In: *The Journal of Adhesion* 95.5-7 (2019), pp. 385–404.

[12] A. Ilioni et al. "A viscoelastic-viscoplastic model to describe creep and strain rate effects on the mechanical behaviour of adhesively-bonded assemblies". In: *International Journal of Adhesion and Adhesives* 82 (2018), pp. 184–195. DOI: 10.1016/j.ijadhadh.2017.12.003.

[13] R. D. Adams. *Adhesive bonding science, technology and applications*. Elsevier, 2005.

[14] Lucas F.M. da Silva and R.D. Adams. "Joint strength predictions for adhesive joints to be used over a wide temperature range". In: *International Journal of Adhesion and Adhesives* 27.5 (2007), pp. 362–379. DOI: 10.1016/j.ijadhadh.2006.09.007.

[15] R.D. Adams et al. "The effect of temperature on the strength of adhesive joints". In: *International Journal of Adhesion and Adhesives* 12.3 (1992), pp. 185–190. DOI: 10.1016/0143-7496(92)90052-W.

[16] CBG Brito, RCM Sales, and MV Donadon. "Effects of temperature and moisture on the fracture behaviour of composite adhesive joints". In: *International Journal of Adhesion and Adhesives* 100 (2020), p. 102607.

[17] RL Fernandes, MFSF De Moura, and RDF Moreira. "Effect of temperature on pure modes I and II fracture behavior of composite bonded joints". In: *Composites Part B: Engineering* 96 (2016), pp. 35–44.

[18] J Moller et al. "Influence of the temperature on the fracture energy of a methacrylate adhesive for mining applications". In: *Applied Adhesion Science* 3.1 (2015), pp. 1–13.

[19] Woo Lim and Hlroshl Mizumachi. "Fracture Toughness of Adhesive Joints. II. Temperature and Rate Dependencies of Mode I Fracture Toughness and Adhesive Tensile Strength". In: *Journal of Applied Polymer Science* 57 (1995), pp. 55–61.

[20] Won Woo Lim and Hiroshi Mizumachi. "Fracture toughness of adhesive joints. III. Temperature and rate dependencies of mode II fracture toughness and adhesive shear strength". In: *Journal of applied polymer science* 63.7 (1997), pp. 835–841.

[21] G Stamoulis and N Carrere. "Investigating the influence of material non-linearity in the fracture properties of ductile adhesives submitted to mixed-mode loading". In: *Engineering Fracture Mechanics* 179 (2017), pp. 260–271. DOI: 10.1016/j.engfracmech.2017.04.017.

[22] J Y Cognard, L Sohier, and P Davies. "A modified Arcan test to analyze the behavior of composites and their assemblies under out-of-plane loadings". In: *Composites Part A* 42 (2011), pp. 111–121. DOI: 10.1016/j.compositesa.2010.10.012.

[23] G Stamoulis et al. "Investigating the fracture behavior of adhesively bonded metallic joints using the Arcan fixture". In: *International Journal of Adhesion & Adhesives* 66 (2016), pp. 147–159. DOI: 10.1016/j.ijadhadh.2016.01.001.

[24] G. Stamoulis and N. Carrere. "Linear elastic analysis of the loading rate dependency of the fracture properties of structural adhesives in the mixed mode I+II plane". In: *Engineering Fracture Mechanics* (2020). DOI: 10.1016/j.engfracmech.2019.106840.

[25] John H. Crews and James R. Reeder. *A mixed-mode bending apparatus for delamination testing*. Tech. rep. 1988.

[26] M. F. Kanninen and C. H. Popelar. *Advanced Fracture Mechanics*. Oxford University Press, 1985.

[27] J.R. Rice. "A Path Independent Integral and the Approximate Analysis of Strain Concentration by Notches and Cracks". In: *J. Appl. Mech* 35.2 (1968), pp. 379–386. DOI: 10.1115/1.3601206.

[28] G. Cherepanov. "Crack propagation in continuous media PMM vol. 31, no. 3, 1967, pp. 476-488". In: *Journal of Applied Mathematics and Mechanics* 31 (1967), pp. 503–512. DOI: 10.1016/0021-8928(67)90034-2.

[29] J. D. Eshelby. "The Force on an Elastic Singularity". In: *Philosophical Transactions of the Royal Society A: Mathematical, Physical and Engineering Sciences* 244.877 (1951), pp. 87–112. DOI: 10.1098/rsta.1951.0016.

[30] Abaqus Inc. *Abaqus 2017 User's Manual*. Dassault Systèmes Simulia Corp, 2017.

[31] J.A. Nelder and RA Mead. "A Simplex Method for Function Minimization Comput". In: *The Computer Journal* 7 (Jan. 1965). DOI: 10.1093/comjnl/7.4.308.

[32] Jeffrey C. Lagarias et al. "Convergence Properties of the Nelder-Mead Simplex Method in Low Dimensions". In: *SIAM Journal on Optimization* 9.1 (1998), pp. 112–147. DOI: 10.1137/S1052623496303470.

[33] Xiao-Jing Gong and Malk Benzeggagh. "Mixed mode interlaminar fracture toughness of unidirectional glass/epoxy composite". In: *Composite Materials: Fatigue and Fracture: Fifth Volume*. ASTM International, 1995.

[34] M L Benzeggagh and M Kenane. "Measurement of mixed-mode delamination fracture toughness of unidirectional glass/epoxy composites with mixed-mode bending apparatus". In: *Composites Science and Technology* 56 (1996), pp. 439–449.

[35] Stephan Marzi, Anders Biel, and Ulf Stigh. "On experimental methods to investigate the effect of layer thickness on the fracture behavior of adhesively bonded joints". In: *International Journal of Adhesion and Adhesives* 31 (2011), pp. 840–850. DOI: 10.1016/j.ijadhadh.2011.08.004.

[36] Michael A Sutton et al. "Development and application of a crack tip opening displacement-based mixed mode fracture criterion". In: *International Journal of Solids and Structures* 37 (1999), pp. 3591–3618.

[37] Michael A Sutton et al. "A combined modeling-experimental study of the crack opening displacement fracture criterion for characterization of stable crack growth under mixed mode I/II loading in thin sheet materials". In: *Engineering Fracture Mechanics* 66 (2000), pp. 171–185.

[38] E Fagerholt et al. "Experimental and numerical investigation of fracture in a cast aluminium alloy". In: *International Journal of Solids and Structures* 47 (2010), pp. 3352–3365. DOI: 10.1016/j.ijsolstr.2010.08.013.

[39] H A Richard, B Schramm, and N.-H Schirmeisen. "Cracks on Mixed Mode loading - Theories, experiments, simulations". In: *International Journal of Fatigue* 62 (2014), pp. 93–103. DOI: 10.1016/j.ijfatigue.2013.06.019.

[40] Robert A Jurf and R Byron Pipes. "Interlaminar Fracture of Composite Materials". In: *Journal of Composite Materials* 16.5 (1982), pp. 386–394.

[41] R Créac'hcadec et al. "A stress concentration-free bonded arcan tensile compression shear test specimen for the evaluation of adhesive mechanical response". In: *International Journal of Adhesion & Adhesives* 61 (2015), pp. 81–92. DOI: 10.1016/j.ijadhadh.2015.05.003.

[42] L. Alfonso, C. Badulescu, and N. Carrere. "Use of the modified Arcan fixture to study the strength of bonded assemblies for automotive applications". In: *International Journal of Adhesion and Adhesives* 80 (2018), pp. 104–114. DOI: 10.1016/j.ijadhadh.2017.09.014.

[43] Jean-Yves Cognard et al. "Analysis of the nonlinear behavior of adhesives in bonded assemblies—Comparison of TAST and Arcan tests". In: *International Journal of Adhesion and Adhesives* 28.8 (2008), pp. 393–404.

[44] J. Moller et al. "Influence of the temperature on the fracture energy of a methacrylate adhesive for mining applications". In: *Applied Adhesion Science* 3.1 (2015), p. 14. DOI: 10.1186/s40563-015-0041-5.